UNIVERSITY OF OKLAHOMA

GRADUATE COLLEGE

NOCTURNAL ASCENT AND LOW-LEVEL JET IN A BAROCLINIC ZONE

A THESIS

SUBMITTED TO THE GRADUATE FACULTY

in partial fulfillment of the requirements for the

Degree of

MASTER OF SCIENCE IN METEOROLOGY

By

MATHEUS BEZERRA GOMES
Norman, Oklahoma
2022

NOCTURNAL ASCENT AND LOW-LEVEL JET IN A BAROCLINIC ZONE

A THESIS APPROVED FOR THE
SCHOOL OF METEOROLOGY

BY THE COMMITTEE CONSISTING OF

Dr. David Parsons, Chair

Dr. Alan Shapiro, Co-Chair

Dr. Scott Salesky

Acknowledgements

Table of Contents

ABSTRACT

A remarkable feature of the regional climatology of the central United States and the Great Plains is the existence of a nocturnal maximum in convective rainfall during the warm season. This study follows up the work of Shapiro et al. (2018; hereafter S18), in which a linear theory predicts weak but persistent ascent in the nocturnal boundary layer in baroclinic environments such as the United States Great Plains. In the S18 theory, the sudden decay of dry-convective mixing in the convective boundary layer at sunset triggers inertia-gravity waves as well as a Blackadar (1957)-like nocturnal low-level jet. For conditions typical of broad warm-season surface-based baroclinic zones extending over one or more Great Plains states, the theory predicts that air parcels in the ascent phase of the wave can rise 500 m - 1 km in 6 hours. Such large displacements may promote convective initiation and play a role in that region's well-known nocturnal maximum in convective rainfall. In the present study, the CM1 numerical model (Cloud Model 1, developed at NCAR by George Bryan) is used to examine whether the main predictions from the S18 ascent/jet theory arise in a more realistic setting. Specifically, in these simulations, the non-linear terms in the governing equations are retained, and the sudden and total shutdown of turbulence at sunset is replaced by a more realistic evening transition. The first sets of experiments focus on generating nocturnal low-level jets in a barotropic environment [no horizontal temperature gradient; free-atmosphere geostrophic wind is constant and southerly at 10 m s^{-1}] and testing the sensitivity of those jets to a few different parameters. The resulting jets are Blackadar-like, tend to be stronger when the boundary layer is shallower and decrease in strength as the latitude increases ranging from 30°N to 45°N. After confirming that Blackadar-like nocturnal low-level jets can be generated by CM1 when run in a barotropic mode, experiments focused on the impact of baroclinicity. A baroclinic zone arises gradually in the CM1-simulated boundary layer over the course of a 4-day integration period mostly through a temporally constant prescribed deficit in the moisture flux at the surface (a Gaussian function of x, with user-specified amplitude and length scale) which causes greater daytime heating in the center of the domain than in the region outside the baroclinic zone. Aspects of the inertia-gravity wave response predicted in S18 are present in all the simulations. In particular, the main zone of ascent that develops after the evening transition is found to slowly descend with time. The peak vertical velocity and duration of the ascent are qualitatively similar to what is predicted by the S18 theory, however the onset of the ascent is generally earlier than predicted in S18. Unlike S18, the peak vertical velocity increases as the free-atmosphere geostrophic wind gets weaker. This discrepancy may likely reflect the fact that S18 does not retain non-linear terms in the governing equations.

1. Introduction

There is a well-documented nocturnal maximum in rainfall in the Great Plains of the United States during the warm season (Wallace 1975, Dai et al. 1999, Tuttle and Davis 2006, Carbone and Tuttle 2008). This rainfall benefits agriculture, but is associated with severe weather (Maddox et al. 1979, Jirak and Cotton 2007). Numerical models routinely have problems forecasting nocturnal rainfall and the intensity of nocturnal rainfall events in the Great Plains (Davies et al. 2003, Lee et al. 2008, Song et al. 2013). Climate models also have problems capturing nocturnal precipitation peaks associated with elevated convection and propagating mesoscale convective systems in different regions of the world (Tang et al. 2021). Several studies have attempted to explain the nocturnal maximum in rainfall, but, because of the variety of mechanisms capable of generating nocturnal convection, none have managed to conclusively show why such a maximum exists. Such mechanisms include the Mountain-Plains Solenoid (MPS) circulation, potential vorticity (PV) disturbances created by the elevated terrain to the west, easterly propagating convection that forms in the lee of the Rockies, elevated ascent associated with elevated convergent layers, quasi-geostrophic (QG) aided ascent, gravity waves, bores, the nocturnal low-level jet (LLJ) and baroclinically generated ascent in the presence of warm tongues (to be discussed later). Each of these mechanisms have a still unknown degree of contribution to the above-mentioned nocturnal rainfall maximum when compared to the other mechanisms. It is also unclear whether some of them even contribute to nocturnal rainfall.

The MPS is a circulation characterized by alternating phases of ascent (upslope flow) and descent (downslope flow) in the Great Plains caused by the heating of the Great Plains slope. Using Rapid Update Cycle (RUC) data, Carbone and Tuttle (2008) documented a MPS circulation characterized by afternoon ascent (associated with upslope flow) in the order of 4-8 cm s^{-1} near the Continental Divide and descent (associated with downslope flow) in the order of 1-2 cm s^{-1} over a broad area centered in the Great Plains. At night, the circulation reverses, resulting in an ascent of 1-2 cm s^{-1} in the Great Plains and descent of 3-6 cm s^{-1} in the mountains [Figure 9 from Carbone and Tuttle (2008)]. This circulation is consistent with the nocturnal maximum in convection in the Great Plains given its nocturnal ascent phase of 1-2 cm s^{-1} over the plains.

Another mechanism that possibly contributes to the nocturnal rainfall maximum during the warm season in the Great Plains are propagating convective systems. Using radar data, Carbone and Tuttle (2008) determined that 60% of the total rainfall in the warm (JJA) season in the central United States occurs because of easterly propagating systems. Most of them originate due to sensible heating over elevated terrain near the Continental Divide and propagate east. Tuttle and Davies (2006) used radar data averaged over the 1998-2002 warm season to show that there is a nocturnal maximum in convection in the Great Plains region around 0800 UTC. This convection partly originates from propagating organized systems from the west and some is partly generated in-situ. It's possible that the MPS circulation contributes to the existence of easterly propagating systems, but it's still unclear how often the MPS circulation contributes to the generation and if it aids in the maintenance of easterly propagating systems.

Using radar and surface data from 1996 to 2015, Reif and Bluestein (2018) documented that about 25% of the nocturnal convection initiation events in the Great Plains warm season occurred without any nearby surface boundaries. The study separately analyzed four of those events to look for common initiation mechanisms. It was found that the LLJ, elevated ascent associated with elevated convergent layers, gravity waves and QG aided ascent were possible candidates for convection initiation.

Reif and Bluestein (2018) also noted that that PV anomalies generated in the lee of the Rockies during the late afternoon/early evening due to latent heat release from convection and solar insolation on locally high terrain (Hoskins et al. 1985, Li and Smith 2010) could move 500 km during a period of 9 hours into central Kansas/Nebraska. The weak ascent of around 1 cm s^{-1} associated with these PV anomalies (Raymond and Jiang 1990) could be enough to lift parcels into their level of free convection when combined with other lifting mechanisms.

Wilson and Roberts (2006) analyzed International H$_2$O project (IHOP) data (Weckwerth et al. 2004) to conclude that afternoon storm initiation episodes were primarily surface based while nocturnal storm initiation episodes were primarily elevated. The cause of many of the elevated initiations during IHOP appeared to be associated with mesoscale or synoptic convergence or confluence at midlevels (900-600 hPa) coupled with an abundance of midlevel instability. Twenty bores occurring in 15 days were also analyzed as potential convection catalysts. It was concluded that although bores occur frequently at night, they played only a very small role in initiating nocturnal thunderstorms.

The nocturnal low-level jet (LLJ) is also an important mechanism that contributes to the maintenance and possibly the generation of nocturnal convection in the Great Plains (Wallace 1975, Tuttle and Davis 2006, Carbone and Tuttle 2008). However, given the importance that LLJs play in this study it is interesting to first understand general aspects of the LLJ before understanding their relation to convection. LLJs are a boundary layer phenomena that consist of a wind speed increase that begins during the afternoon-evening transition and consequent generation of a supergeostrophic wind maximum in the nocturnal boundary layer. The LLJ often resides (but with large variability) above the stable boundary layer (Blackadar 1957, Bonner 1968, Whiteman et al. 1997, Shapiro and Fedorovich 2009) and peaks around 400-1000 m above ground level (AGL) (Bonner 1968, Mitchell et al. 1995, Whiteman et al. 1997, Song et al. 2005, Walters et al. 2014). The LLJ starts to form when buoyancy generated turbulence in the boundary layer starts to decay in the late afternoon, reaches maximum intensity typically shortly after local midnight (Bonner 1968, Arritt et al. 1997, Whiteman et al. 1997, Song et al. 2005) and then starts to get mixed out with the onset of boundary layer mixing driven by solar heating in the morning. LLJs are stronger in fair-weather conditions, which maximize the contrast in turbulent intensity between day and night. According to the Blackadar theory, the LLJ can have any direction, as long as there is an initial geostrophic wind present (Parish and Oolman 2010). The LLJ is important for the generation of wind energy, but turbulence and wind shear associated with it can have negative effects on wind turbines (Storm et al. 2009).

LLJs can occur in any region of the world (Salio et al. 2002, Marengo et al. 2004, Phan et al. 2008, Baas et al. 2009, Fiedler et al. 2013), but this study will focus on the Great Plains of the United States, where LLJs have been extensively documented during the warm season (Bonner

1968, Whiteman et al. 1997). They occur more frequent roughly in a region corresponding to the states of Texas, Oklahoma, Kansas, Nebraska and South Dakota, with a peak occurrence in western Oklahoma (Bonner 1968, Mitchell et al. 1995). Consistent with the Blackadar (1957) theory, given the predominant southerly geostrophic wind in the Great Plains during the warm season, the LLJ is predominantly from the south (Bonner 1968, Mitchell et al. 1995, Parish and Oolman 2010). Northerly LLJs are less common but are typically associated with cold fronts and occur independently of the time of day (Bonner 1968, Whiteman et al. 1997).

The dynamics of the LLJ started to become more clearly understood with the development of the Blackadar (1957) inertial oscillation theory. Blackadar describes the LLJ as an inviscid inertial oscillation of the ageostrophic component of the wind which develops in response to the shutdown of turbulence in the afternoon-evening transition. If the geostrophic wind is constant in time then the magnitude of the ageostrophic component of the wind at each height is constant after sunset, but its direction oscillates around the value of the geostrophic wind. When the ageostrophic wind direction aligns with the geostrophic wind direction (usually a few hours after midnight), the LLJ reaches its maximum intensity. However, supergeostrophic winds are observed prior to that. Because the highest values of the ageostrophic winds are found at low levels and the ageostrophic wind rotates with time to eventually produce supergeostrophic winds, the stronger LLJ winds will be found at low levels. The Blackdar (1957) theory assumes that the turbulence completely shuts down at sunset (eddy viscosity and eddy diffusivity go to zero at sunset), but that doesn't happen in the real atmosphere. Instead, their values tend to decrease during the evening transition, but never go to zero. In order to address this issue, Buajitti and Blackdar (1957) included varying values of eddy viscosity with time and height in the Blackadar theory. However, this model still could not explain the amplitude and shape of the diurnal wind oscillation.

Given that the Blackdar model could not explain why the LLJ is concentrated in the plains east of the Rockies and with a strong southerly component, Holton (1967) created an analytical model that attempts to address this issue. In the Holton model, a weak nocturnal wind maximum is generated by a slope that is evenly heated during the day (no along-slope buoyancy gradient). The baroclinicity that develops between air that is close to the heated/cooled slope and air further east at the same height generates an easterly/westerly pressure gradient force (PGF) during the day/night which creates a wind oscillation in the geostrophic wind. However, the nocturnal LLJ-like wind maxima produced by the Holton model is unable to replicate the structure and phase of the typical LLJ in detail.

Bonner and Peagle (1970) used an analytical model created by Peagle (1970) capable of producing LLJs under three different scenarios: time dependent eddy viscosity and geostrophic wind that was assumed to be a function of height only; constant eddy viscosity and variable geostrophic wind (with respect to time and height); time dependent eddy viscosity and variable geostrophic wind (with time and height). However, unlike the Holton (1967) model, the variation in the geostrophic wind is prescribed, as there is no thermodynamic equation and the coordinate system is not modified to include the presence of a slope. This model is capable of replicating with some degree of accuracy the major features of the LLJ when diurnally varying

3

eddy viscosity and geostrophic wind are included, such as the structure of the oscillation, time of maximum intensity and the maximum intensity of the jet.

Shapiro and Fedorovich (2009) also attempted to combine some aspects of the Blackdar and Holton mechanisms in an inviscid analytical model. Their model includes a slope with the x-coordinate pointing east and down the slope and the y-coordinate pointing across the slope and to the north. The solution starts at sunset, when turbulence is assumed to completely shut down. Therefore, there are no turbulence terms in the equations of motion. The solution only pertains to the nighttime flow. It is found that increasing both the slope angle and stratification causes a reduction in the amplitude of the oscillation. The upslope advection of potential temperature results in negative values of buoyancy, which damps the amplitude of the oscillation. Lower values of the initial V wind (larger ageostrophic wind) cause an increase in the amplitude of the oscillation and consequently larger values of V_{max}, as is expected from the Blackdar (1957) theory. Larger values of initial buoyancy also result in larger oscillation amplitudes and a larger V_{max}. The amplitude of the oscillation is maximized for a slope angle of approximately 0.3 degrees. The introduction of a slope leads to the idea of a tilted boundary layer (boundary layer is parallel to the slope). The result is that parcels close to the ground have positive values of initial buoyancy because the air closer to the slope will be warmer than air further east in the same altitude. Since larger initial values of buoyancy lead to stronger jets, the existence of a tilted boundary layer leads to stronger jets.

Shapiro et al. (2016; hereafter S16) improved on the Shapiro and Fedorovich (2009) model by adding several missing features to it. As in the Shapiro and Fedorovich (2009) model, a background constant southerly geostrophic wind is imposed and flows parallel to a slope. The surface buoyancy varies as a piecewise-linear function of time to represent the diurnal cycle. The turbulent diffusivities vary as a piecewise constant function of time, with fixed values for day and night. Diurnally periodic solutions are obtained for all variables. It was found that the intensity of the LLJ is enhanced by larger values of the background southerly geostrophic wind, larger values of peak positive surface buoyancy and an increasing ratio of day-to-night diffusivities (large daytime diffusivity and smaller nighttime diffusivity). Klein et al. (2016) also found that the relative LLJ strength depends on the degree of change in atmospheric stability and turbulence intensity during the early evening transition. The results of the S16 theory are remarkably similar to LLJ observations: The shape of the oscillation, maximum LLJ wind speed values, time of maximum LLJ winds, height of the LLJ, etc. all come very close to real values. Similarly to the Shapiro and Fedorovich (2009) model, the LLJ strength is maximized for a slope angle of approximately 0.2 degrees, characteristic of the Great Plains.

Gebauer and Shapiro (2019) noted that not only a constant along slope positive buoyancy value can generate an increase in the geostrophic wind parallel to the slope, but also an along slope buoyancy gradient. Uneven heating of a slope (or even flat terrain) generates a buoyancy gradient (baroclinicity) that strengthens the geostrophic wind parallel to the slope.

Shapiro et al. (2022; hereafter S22) also explores the effects of a buoyancy gradient in the strength of the LLJ trough an analytical model, but without introducing a slope. The model includes a diurnally periodic surface buoyancy gradient in the east-west direction in the presence of a 10 m s^{-1} southerly free-atmosphere geostrophic wind. The eddy viscosity and

diffusivity also vary periodically according to a piecewise constant function, with an abrupt increase (decrease) at sunrise (sunset). The solutions for all variables are periodic as in S16 and can produce strong jets from typical atmospheric conditions. Removing the free-atmosphere geostrophic wind and keeping the buoyancy gradient (surface buoyancy decreasing at a rate of -0.2 m s^{-2} for every 1000 km) results in a jet that is 60% weaker, while removing the buoyancy gradient and keeping the 10 m s^{-1} southerly geostrophic wind (Blackdar jet) results in a 40% weaker jet (all other parameters can be found in table 1 and 2 of S22). In the analytical model run mentioned above without the buoyancy gradient (which produces a Blackdar jet), the intensity of the jet was stronger when there was a larger decrease in turbulence at sunset, which is consistent with S16 and also with Klein et al. (2016). When ECMWF (European Centre for Medium-Range Weather Forecasts) Reanalysis v5 (ERA5) wind and virtual potential temperature data (to estimate the surface buoyancy gradient) from an afternoon immediately prior to a LLJ night in the Great Plains was fed into the analytical model, the model reproduced the peak values of u, v and wind speed, as well as the heights and times of these maxima with a high degree of accuracy (results verified using doppler lidar winds from a location within the baroclinic zone near Lamont, OK).

The LLJ contributes to the generation of convection in many different ways: It can aid in the formation of an unstable environment by advecting low-level moist and warm air from the south (Beebe and Bates 1955, Trier and Parsons 1993, Reif and Bluestein 2017, Blake et al. 2017, Gebauer et al. 2018, Reif and Bluestein 2018, Parsons et al. 2019, Smith et al. 2019). Convergence mostly in the northern terminus of the jet (Beebe and Bates 1955, Bonner 1966, Trier and Parsons 1993, Tuttle and Davis, 2006), to the left of the jet axis (Beebe and Bates 1955, Bonner 1966, Walters and Winkler, 2001) and to the right of the jet axis (Pu and Dickinson 2014, Gebauer et al. 2018) can help initiate and maintain convection. Convergence generated by heterogeneity in the LLJ flow (Gebauer et al. 2018, Smith et al. 2019) is one mechanism that can lift parcels to their level of free convection. The LLJ can advect warm and moist air over a boundary, such as a cold, warm, quasi-stationary front or a dryline, aiding in the generation of convection (Trier and Parsons 1993, Reif and Bluestein 2017). Veering of the LLJ winds with increasing height (winds turning from south to southwest) happening first in the western part of the jet and later at night in the eastern part of the jet creates regions of convergence that can potentially generate convection (Smith et al 2019).

Several mechanisms can aid in the generation of nocturnal convection in the Great Plains, some more well-documented than others. This study will focus on a new mechanism proposed by S18, which is intimately linked to the LLJ. S18 developed an analytical model in which weak but persistent ascent is generated when dry-convective mixing decays at sunset in a convective boundary layer (which also generates a Blackadar-like inertial oscillation) in the presence of a warm tongue. Similar to Shapiro and Fedorovich (2009), the model is initialized at sunset, which removes the need for turbulence terms in the equations of motion. Given that there are no turbulent terms, it is unfeasible for the analytical model to be applied for daytime flow. The initial conditions (at sunset) include a free-atmosphere southerly geostrophic wind of 10 m s^{-1} and a boundary layer that is well mixed. The potential temperature and the initial V wind are piecewise functions of z, with constant values in the boundary layer and discontinuities at the surface and at the capping inversion. The initial V wind in the boundary layer is set as a fraction

of the free-atmosphere geostrophic V wind component. The initial potential temperature in the boundary layer follows a periodic cosine function in the east-west direction with higher values towards the center, which creates a warm tongue in the center (see figure 5 from S18). The boundary layer is initially well mixed.

For the parameters specified in table 1 of S18 (λ = 1000 km case), a gravity wave is generated in the center of the domain upon analytical model initialization, with associated vertical motions reaching up to 5 cm s^{-1} approximately 2.5-3 hours after sunset. The ascent and descent phases of the wave each last approximately 7 hours and a parcel located near the half-depth of the boundary layer rises approximately 750 m during the ascent phase. Such magnitudes of parcel displacements can potentially contribute to the generation of nocturnal convection.

Because turbulence shuts down after sunset and there is no slope in the model, a Blackadar type LLJ develops. However, this jet is stronger because of baroclinic effects (potential temperature and buoyancy increase towards the center of the domain). In the presence of the warm tongue, the shutdown of turbulence induces a convergent/divergent circulation. Although the ascent rates produced by the S18 model are capable of aiding in the generation of convection, several limiting assumptions are made, that may restrict the applicability of the results in a more realistic setting. Some examples are: There are no advection terms in the equations of motion, the piecewise treatment of the wind and potential temperature in the boundary layer is quite unrealistic, the sudden shutdown of turbulence at sunset doesn't happen in the real atmosphere (what is observed is a gradual decrease to small but non-zero values), there is no slope and the warm tongue in the model is very different from warm tongues found in the Great Plains (it is periodic on an infinite domain). To further complicate matters, the ascent rates produced by the model are too weak to be measured directly by real observing systems. In order to verify if ascent was occurring as predicted by the model in days with a LLJ and a warm tongue, the displacement of layered structures (WV-DIAL relative backscatter, 449 MHz profiler signal-to-noise ratio, MPL relative backscatter and CL31 ceilometer backscatter) in the atmosphere was used as a proxy for vertical motion in the S18 study.

Together with the S18 model, there are several other mechanisms that possibly contribute to the warm season nocturnal maximum in rainfall in the Great Plains. Those mechanisms include, but are not limited to: LLJs, the MPS, easterly propagation of convection that formed in the lee of the Rockies, bores, PV disturbances, QG aided ascent and elevated convergence layers.

Given the not insignificant parcel displacements generated by the S18 theory, the current study will use the CM1 numerical model (Cloud Model 1, developed at NCAR by George Bryan) to examine whether the main predictions from the S18 ascent/jet theory arise in a more realistic setting. Specifically, in these simulations, the non-linear terms in the governing equations are retained, the sudden and total shutdown of turbulence at sunset is replaced by a more realistic evening transition and the structure of the boundary layer is kept closer to what is observed in the Great Plains.

2. Methods

Version 20.2 of idealized 3D numerical model CM1 (Bryan and Fritsch 2002, Bryan and Rotunno 2009) was used to conduct different idealized mesoscale simulations. CM1 is a three-dimensional, non-hydrostatic, non-linear, time-dependent numerical model designed for idealized studies of atmospheric phenomena. The velocity equations are:

$$\frac{\partial u}{\partial t} + c_p \theta_p \frac{\partial \pi'}{\partial x} = ADV(u) + fv + P_u + T_u + D_u + N_u \tag{1}$$

$$\frac{\partial v}{\partial t} + c_p \theta_p \frac{\partial \pi'}{\partial y} = ADV(v) - fu + P_v + T_v + D_v + N_v \tag{2}$$

$$\frac{\partial w}{\partial t} + c_p \theta_p \frac{\partial \pi'}{\partial z} = ADV(w) + B + T_w + D_w + N_w \tag{3}$$

In equations (1), (2) and (3), the π' term is a nondimensional pressure, c_p is the specific heat of dry air at constant pressure, f is the Coriolis parameter, ADV is and advection operator, the P terms represent specified large-scale pressure gradients, the D terms represent optional artificial diffusion, the T terms represent tendencies from subgrid turbulence, the N terms represent Newtonian relaxation (i.e. Rayleigh Damping) and B is buoyancy. The θ_p term is density potential temperature, which is equal to:

$$\theta \left(\frac{1 + q_v/\varepsilon}{1 + q_v + q_l + q_i} \right) \tag{4}$$

In equation (4), q_v is the water vapor mixing ratio, q_l is the mixing ratio of liquid water and q_i is the mixing ratio of ice.

The T terms are:

$$T_u = \frac{1}{\rho} \left(\frac{\partial \tau_{11}}{\partial x} + \frac{\partial \tau_{12}}{\partial y} + \frac{\partial \tau_{13}}{\partial z} \right) \tag{5}$$

$$T_v = \frac{1}{\rho} \left(\frac{\partial \tau_{12}}{\partial x} + \frac{\partial \tau_{22}}{\partial y} + \frac{\partial \tau_{23}}{\partial z} \right) \tag{6}$$

$$T_w = \frac{1}{\rho} \left(\frac{\partial \tau_{13}}{\partial x} + \frac{\partial \tau_{23}}{\partial y} + \frac{\partial \tau_{33}}{\partial z} \right) \tag{7}$$

The τ_{ij} terms are the subgrid stress terms.

The CM1 model always applies the same latitude and longitude to the whole domain, which were chosen to be 36.68N, -98.35W. The latitude and longitude correspond to a location in Central Oklahoma but are only used to calculate the intensity of the incoming shortwave radiation (the Coriolis parameter is set separately to $8.4 \times 10^{-5}\,\text{s}^{-1}$). The starting date for all

7

simulations (which only gets used to calculate the intensity of the incoming solar radiation and the duration of the day) was chosen to be June 10th. Simulations last 4-7 days, starting in day 1 at 0030 LST. The sunrise (0530 LST) and sunset (2030 LST) times were chosen based on figure 1.

The geostrophic wind is southerly at 10 m s^{-1} everywhere in the domain and the potential temperature profile is taken from a Purcell, OK rawinsonde profile (figure 2) from the 4th of June 2002 at 0530 UTC (which corresponds to 0030 LST) observed during IHOP. The initial moisture profile is not representative of the Purcell sounding; almost all the moisture is removed because even small amounts of moisture cause convection initiation (figure 3), which disrupts the boundary layer and flow structure. Small amounts of moisture also lead to stratiform cloud formation, which disrupts the radiative budgets. A sixth order diffusion scheme that filters small scale fluctuations smaller than approximately six times the grid spacing (Knievel et al. 2007) is used in order to prevent instabilities from forming in the boundary layer [included in the D terms in equations (1), (2) and (3)]. CM1 allows the user to choose a diffusion coefficient, which was set to 0.2. CM1 allows users to choose between different "LANDUSE" types, which include "Irrigated Cropland", "Grassland", "Desert", etc. The chosen "LANDUSE" type varies from one simulation to the other (specified in sections 3 and 4).

A 2-D (x-z) domain with very large horizontal dimension (12,960 km) is used in order for gravity waves generated in the center not to come back to their origin and cause disruptions. There are 3 points in the y direction (in order to use distributed memory during model execution) but all fields are homogeneous at all times in the y direction, resulting in simulations that behave as 2-D simulations (x-z). The north and south boundaries are periodic (what leaves the domain from one boundary comes back through the opposite boundary) which is a requirement for 1-D and 2-D simulations. The east and west boundaries are also periodic. The height of the domain is 14 km, with a Rayleigh damping zone at 12 km in order to damp gravity waves. Grid sizes of 20 m in the vertical (20 m in the lowest 3 km and stretched up to 349 m at the top of the domain) and 20 km in the horizontal were used. The Yonsei Univeristy (YSU) boundary layer parameterization was used (Hong et al. 2006), together with a revised version of the surface layer scheme from the WRF model (Jimenez et al. 2012). The YSU parameterization is a revision of the vertical diffusion package from the Medium-Range Forecast (MRF) model (Hong and Pan 1996) that includes nonlocal turbulent mixing in the boundary layer. Its most important modification is the inclusion of explicit treatment of the entrainment processes in the boundary layer. The use of a boundary layer parameterization implies that turbulent eddies are too small to be resolved on grid and therefore need to be parameterized. All simulations use Reynolds-averaged Navier-Stokes equations (mesoscale modeling with planetary boundary layer parameterizations in CM1).

3. Barotropic Simulations

a. Reference Blackadar jet run

A flat lower boundary is used in this simulation in order to test the model's performance in simulating the Blackadar mechanism alone. Since no perturbations are added to the initial

8

state, all variables are horizontally homogeneous at all times (essentially a 1-D simulation). As a result, there is no vertical motion or large-scale turbulence forming in the domain. Since the flow is independent of x and y, the horizontal grid spacing is irrelevant. However, horizontal grids of 20 km were still used (as was described in the methods section). Turbulence occurs in subgrid-scales and its effects on the larger scale flow are parameterized. A timestep of 20 s is used. The "LANDUSE" type was chosen to be grassland.

Figure 4 shows the development of the LLJ over a 5-day period. It is seen that the LLJ peaks around 2330 LST on each night, which is slightly earlier than typical Great Plains observations of Buajitti and Blackadar (1957), Mitchell et al. (1995), Arritt et al. (1997) and Whiteman et al. (1997). However, the numerical setting used in this simulation is very different from the typical Great Plains environment. The height of the boundary layer (figure 4) grows every day, which is a consequence of the intensity and duration of the incoming solar radiation (large for a summer day) added to the lack of convection or cloud formation. The boundary layer grows to almost 4 km in the sixth day of the simulation, which could be from the fact that the YSU scheme is producing unrealistically tall boundary layers. Clouds form in the end of the fifth day of the simulation, which makes the results unsuitable for analysis of dry LLJs.

An interesting feature is that the peak wind speed (the maximum value is 14.40 m s^{-1} in the second day of the simulation) in the LLJ is almost constant with height in most of the boundary layer (there is a small non-uniformity close to the surface that will be discussed later). This is inconsistent with some observational studies (Bonner 1968, Whiteman et al. 1997, Klein et al. 2016), which have reported that the LLJ has a more distinct peak around 400-1000 m. However, it is possible that none of the LLJs in these observational studies are purely barotropic jets.

An explanation as to why the wind speed in the core of the LLJ is constant with height in most of the boundary can also be found in figure 4: the wind speed profile is well mixed and uniform with height in most of the boundary layer at sunset, which according the Blackadar mechanism should generate a jet that is also uniform with height. However, one key difference between the Blackadar mechanism and this reference run is that the effects of turbulence don't decay completely at sunset. Even though the turbulence doesn't decay completely at sunset, it still decays with time but is largely independent of height in the region of the LLJ core, which explains why the LLJ wind speed tends to be uniform with height.

Both the effects of turbulence in the wind field and subgrid scale (i.e. parameterized) turbulent kinetic energy decay too rapidly after sunset (leading to an inertial oscillation that starts earlier), which could potentially explain why the jet peaks earlier than in some observational studies. In the real atmosphere, the turbulence decays more slowly. In this idealized run, the turbulent kinetic energy goes from a maximum value around 270 m^2 s^{-2} to essentially zero in a few hours and remains close to zero during the whole night. Even before sunset the turbulent kinetic energy is almost zero and the "planetary boundary layer (PBL) tendency" term [included in the T terms specified in equations (5), (6) and (7)], which represents the effects of subgrid turbulence in the wind field (figure 5) also goes to zero before sunset. In the real atmosphere,

9

the daytime buoyancy generated turbulence does not decay to zero before sunset (Klein et al. 2016). It is concerning that the effects of turbulence in the boundary layer are negligible even before sunset, which highlights a possible issue with the turbulence parameterization in the YSU scheme.

The strength of the LLJ decreases with each following day (figure 4), which is possibly (if the following logic holds true in the real atmosphere) a consequence of turbulence mixing occurring over a larger depth of air each successive day: During the day, convective mixing brings air from the top of the boundary layer which is flowing at approximately the free-atmosphere geostrophic speed into contact with the ground, where it is forced to slow down (and point towards the direction of the pressure gradient force) due to friction. The convective mixing "spreads" the effects of surface friction over the whole boundary layer, which causes a reduction in the windspeed compared to the geostrophic value (larger ageostrophic wind). If the boundary layer grows taller, the convective mixing has to "spread" the effects of surface friction over a larger depth, effectively diluting it. As a result, the ageostrophic wind in the boundary layer gets weaker with each passing day, leading to a weaker Blackadar LLJ at night. It is unclear if this process is happening in this simulation, but the ageostrophic wind magnitude decreases with each passing day as the height of the boundary layer grows (figure 6).

In addition to the LLJ weakening together with the ageostrophic wind magnitude with each passing day, days with stronger LLJs have stronger ageostrophic wind components at sunset (2030 LST), which is in agreement with the Blackadar theory (figure 6). The "PBL tendency term", which represents the effects of unresolved (subgrid scale) turbulence in the U and V winds does indeed become weaker as the height of the boundary layer grows (not shown), which indicates that the effects of turbulence in the wind field are getting weaker.

An interesting feature of the LLJ produced in this reference run is a small non-uniformity or peak in the V wind at low levels around 0300 LST (figure 7). This peak can also be seen in figure 4 as a tongue of higher wind speeds at low levels that penetrates into an area of lower wind speeds (in purple). This peak results from the Coriolis force (the Coriolis force is $-fu$ and the base PGF is zero in the V equation of motion) being more positive at low levels than at high levels, which causes the V wind above this peak to recede faster than in the peak itself. The Coriolis force is more positive in the area of the peak because the U wind is more negative in this area due to surface friction. A very similar peak in the wind speed is also present in figure 5 from Kumar et al. (2006), which uses a large eddy simulation to study the diurnal cycle on the atmospheric boundary layer.

A similar process happens with the U wind: because the V wind is weaker closer to the ground due to surface friction, the "Coriolis minus base PGF" term

$$fv - fv_0 \tag{8}$$

in the U equation of motion is negative in this area, which essentially creates a peak in the U wind at very low levels, reaching almost - 5 m s^{-1}. The v_0 term in equation (8) represents the V

wind at time = 0. This peak at low levels in the U wind profile is shallower than what is typically observed and is likely a result of the unrealistic inversion that forms during the night (figure 8), which reduces the effectiveness of turbulent mixing in smoothing out the peak. The extreme inversion is likely caused by excessive cooling in a dry environment (most of the moisture was removed from the initial sounding to prevent cloud formation).

The maximum wind speed in the LLJ core was 14.40 m s^{-1} in the second day of the simulation (maximum value out of the all the days), which is weaker than what is usually observed in the Great Plains (Whiteman et al. 1997, Song et al. 2005, Walters at al. 2014), but in agreement with the average wind speed at the level of maximum winds in Mitchell et al. (1995). A weaker jet than what is usually observed in the Great Plains was expected, since the slope effect is not present and there is no along-surface buoyancy gradient (no baroclinicity of any sort). In addition, the geostrophic wind speed is variable in the Great Plains, not constant at 10 m s^{-1}.

An attempt is made to replicate the wind hodograph that results from the Blackadar theory. Figure 9 shows the evolution of the wind in the simulation, starting at 2030 LST of the second day, and ending at 2030 LST of the third day. The magnitude of the ageostrophic wind remains almost constant (circle of constant radius) throughout the whole night and is only disrupted by turbulence in the following day around 1230 LST. The wind at 900 m completes a circle of larger radius than the wind at 1900 m, which indicates that its ageostrophic wind component is larger. Blackadar's theory predicts that heights containing winds with the largest ageostrophic components at sunset will be the heights in which the strongest winds will be found when the LLJ develops. That holds true for heights between 900 m and 1900 m in the simulation. However, for heights below 900 m, extending almost to the ground, the circles almost exactly match the 900 m circle (not shown). This occurs because the winds in the boundary layer are almost constant with height from 400 m-1500 m at sunset, meaning that they have the same initial ageostrophic component.

b. Reference Blackadar jet run with modified starting date

A run with the exact same parameters as the reference Blackadar experiment was conducted with the only difference being the starting date, chosen to be February 10th (in CM1 the starting date only gets used to calculate the incoming solar radiation and the duration of the day). Figure 10 shows the development of the LLJ during the course of nine days and is directly comparable to figure 4. The LLJ tends to peak at around 0030 LST, which is one hour earlier than the reference run. It is slightly stronger than in the reference Blackadar run (the maximum LLJ wind speed out of all the days was 15.20 m s^{-1} compared with 14.40 m s^{-1} in the reference run). This result is surprising, given that in the Great Plains LLJs are less frequent in the cold season and strong LLJs are more common in the warm season (Bonner 1966, Whiteman et al. 1997, Song et al. 2005). A possible explanation is that because the boundary layer is shallower in the February run, the turbulent mixing effect is "spread" out over a smaller column of air, resulting in a stronger low-level ageostrophic wind component before sunset and making the

LLJ stronger. Figure 11 shows that the ageostrophic wind component is larger than in the reference run, but it is unclear whether this increase results from the fact that the boundary layer is shallower than in the reference run. The reduction in the low-level ageostrophic wind component with time in the boundary layer is even more pronounced than in figure 6, which supports the hypothesis that what is causing the jet to weaken is the reduction in the ageostrophic wind caused by the growth of the boundary layer height.

Although the LLJ is stronger in the February run compared to the reference run, the southerly geostrophic wind in the Great Plains is usually weaker in the cold season than in the warm season, which reduces the occurrence of LLJs in the cold season. However, it is possible that the LLJ in the cold season is stronger if the magnitude of the geostrophic wind is not taken into consideration (and assuming all other relevant parameters that affect LLJ strength remain constant).

c. Reference Blackadar jet run with increased surface roughness lengths

Given that an increase in the intensity of the low-level ageostrophic wind component results in a stronger LLJ, a run with a larger value for the surface roughness length (from 0.12 m to 1 m) was conducted. Increasing the size of the roughness elements causes an increase in surface friction and a consequent increase in the magnitude of the ageostrophic wind (not shown). The maximum wind speed of the LLJs that formed in this simulation was 15.95 m s^{-1}, which is slightly stronger than the reference run (14.40 m s^{-1}). This result indicates that a stronger ageostrophic wind magnitude resulting from an increased surface roughness length is related to stronger LLJs. However, the value of 1 m for surface roughness length is possibly unrealistic (the CM1 model assigns a value of 0.8 m for an urban area and built-up land). Using a surface roughness length of 0.8 m results in a maximum LLJ wind speed of 15.75 m s^{-1}.

d. Reference Blackadar jet run with very strong inversion

Given that the simulated Blackadar LLJ was stronger in February than in June (reference run), an additional simulation was conducted with the goal of exploring whether a shallower boundary layer yields a stronger LLJ independently of the intensity of solar heating. This was achieved through the introduction of an unrealistically strong inversion (figure 12). The stronger inversion results in a shallower boundary layer than in the reference run, with slightly stronger LLJs (figure 13). The maximum wind speed in the LLJ core was 15.23 m s^{-1} out of all simulation days. Figure 14 shows that the magnitude of the ageostrophic wind is also stronger than in the reference run. The strongest LLJ day in figure 13 corresponds to the day with the strongest magnitude of ageostrophic wind in the late afternoon/sunset in figure 14, which is in agreement with the Blackadar theory.

e. Reference Blackadar jet run with modified Coriolis parameters

12

Two runs with Coriolis parameters of 7.72×10^{-5} s^{-1} and 1.028×10^{-4} s^{-1} corresponding to locations at latitudes 30°N and 45°N were conducted. All other parameters were kept the same as in the reference run, including the incoming solar radiation.

The maximum LLJ wind speed for the 30°N run is 15.27 m s^{-1}, which is stronger than the reference run. Du and Rotunno (2014) found that the LLJ is stronger at 30°N using an analytical model similar to the Blackadar model but with diurnally varying frictional coefficients. The ageostrophic wind component (figure 15) is stronger in all days when compared to the reference run (which is consistent with a stronger LLJ). The ageostrophic wind magnitude increases everyday together with the intensity of the LLJ, which is the opposite of what happens in the reference Blackadar jet run. This result indicates that the magnitude of the ageostrophic wind in the boundary layer is not necessarily related to the height of the boundary layer and to the effects of turbulent mixing. Shibuya et al. (2014) argued that a resonance-like amplification of the inertial oscillation was observed under the diurnal forcing caused by the turbulent stress at latitudes where the inertial frequency accords with the diurnal frequency and its harmonics. At 30°N, the inertial frequency is 24 hours, which is the same as the diurnal frequency. Therefore, it is possible that a resonance-like amplification such as the one in Shibuya et al. (2014) is causing the magnitude of the ageostrophic wind and the intensity of the LLJ to increase with each passing day.

Compared to the reference Blackadar run, the inertial period $\left(\frac{2\pi}{f}\right)$ is larger for the 30°N run since the percentage of the circle lying between 2030 LST and sunrise is smaller than in the reference run (figure 16). Values after sunrise are not considered because daytime convective turbulence disrupts the inertial oscillation. Because the inertial period is larger at 30°N, the LLJ also peaks later than in the reference run (around 0230 LST). The radius of the oscillation is larger at 900 m than at 1900 m, which is also predicted by the Blackadar theory.

The maximum LLJ wind speed for the 45°N run is 13.41 m s^{-1}, which is weaker than the reference run. A weaker jet at 45°N also occurs in the Du and Rotunno (2014) analytical model. Both the pressure gradient force and Coriolis parameter are larger than the 30°N and reference runs, but it is unclear how that translates into weaker LLJs. The ageostrophic wind component is weaker in all days when compared to the reference run (which is consistent with a weaker LLJ). Unlike the 30°N run, the ageostrophic wind magnitude and the strength of the LLJ decrease with each passing day.

Figure 17 shows that compared to the reference Blackadar run, the inertial period is smaller for this run since the percentage of the circle lying between 2030 LST and sunrise is larger than in the reference run. Values after sunrise are not considered because daytime convective turbulence disrupts the inertial oscillation. The LLJ peaks earlier than in the reference run (around 2230 LST), which is consistent with the smaller inertial period at 45°N. The radius of the oscillation is larger at 900 m than at 1900 m, which is also predicted by the Blackadar theory.

f. Reference Blackadar jet run with very strong inversion and modified Coriolis parameter

In the reference Blackdar run, it was hypothesized that the strength of the LLJ decreases with time because the turbulent mixing gets weaker as the height of the boundary layer grows. This results in a smaller ageostrophic wind component. However, the reference run conducted at 30°N did not follow this behavior; the ageostrophic wind increased as the boundary layer grew taller.

In both the reference run conducted with a starting date of February and the reference run with a very strong inversion, the LLJ was larger in magnitude than in the original reference run. Both these runs had a shallower boundary layer than the original reference run. In order to gain further insight into whether a shallower boundary layer causes an increase in the LLJ strength, an additional run was conducted with the Coriolis parameter calculated as a latitude of 30°N and also with a strong inversion (essentially a combination of the reference run with a very strong inversion and the reference run with modified Coriolis parameters). It is found that the addition of a strong capping inversion makes the LLJ even stronger than the 30°N run (maximum value of 16.18 m s^{-1}). The ageostrophic wind magnitude is also stronger than in the 30°N run (figure 18). Interestingly, the ageostrophic wind magnitude decreases as the height of the boundary layer grows, which did not happen in the 30°N reference run. It is unclear why this happens.

Given this result, it is possible that shallower boundary layers indeed produce stronger LLJs because they are associated with stronger ageostrophic winds. However, it still remains unclear why the ageostrophic wind magnitude increases with time in the 30°N reference run and decreases with time in this run.

g. Reference Blackadar jet run with modified moisture profile

In the reference run, the moisture content in the initial conditions was reduced (compared to the sounding utilized to generate the temperature profile) to prevent the formation of clouds. In this run, the moisture profile in the sounding used to generate the initial temperature profile was not modified. The moisture values are the same as in the values observed in the sounding utilized to initialize the potential temperature profile (figure 19). All the other variables remain the same as in the reference run. The boundary layer grows faster in the first days of the simulation because water vapor is more buoyant than dry air. The nocturnal surface cooling is less extreme which leads to a less shallow inversion near the surface. Because the nocturnal inversion is not as extreme, the shallow U wind peak in figure 7 is not as shallow (figure 20). Instead, the U wind profile close to the surface looks more realistic. The LLJ that develops in the end of the first day of the simulation is weaker than the LLJ that develops in the first day of the reference Blackadar run, possibly because the boundary layer is taller. However, a cloud layer forms in the end of the first day of the simulation, which modifies the radiative budgets, making the results unsuitable for analysis of dry LLJs in the rest of the simulation.

14

4. Baroclinic Simulations

a. Reference baroclinic jet run

The reference baroclinic jet run is similar to the reference Blackadar run, but with the surface layer moisture, albedo and thermal inertia varying laterally according to

$$\text{MAVAIL} = \text{SLMO} - 0.23 \times \exp\left(-x^2/_{\text{DISTANCE}^2}\right) \tag{9}$$

$$\text{ALBEDO} = 0.15 + 0.07 \times \exp\left(-x^2/_{\text{DISTANCE}^2}\right) \tag{10}$$

$$\text{THC} = 0.04 - 0.015 \times \exp\left(-x^2/_{\text{DISTANCE}^2}\right) \text{ Cal cm}^{-1}\text{K}^{-1}\text{s}^{-0.5} \tag{11}$$

The goal of this experiment is to simulate a gradual transition between a forested area in eastern Oklahoma (edges of the computational domain) and semi-arid area in western Oklahoma (center of the computational domain) which is drier than a typical grassland but moister than a barren area (essentially a transition zone between a grassland and a barren area). MAVAIL (soil moisture availability) is a dimensionless parameter which varies from 0 to 1 that CM1 uses to calculate surface moisture fluxes, SLMO is the "LANDUSE" value of surface layer moisture used in the simulation (chosen to be 0.3), THC is thermal inertia, x is the distance to the center of the domain (negative to the left of the center of the domain and positive to the right) and DISTANCE is the *e* folding distance (set to 500 km). The value of 0.3 represents the surface layer moisture value of a forested area according to the CM1 documentation.

Equation (9) results in a moisture drop off from 0.3 to 0.07 as one moves from the edges to the center of the computational domain (figure 21). According to the CM1 documentation, the value of 0.3 represents the surface layer moisture value of a forested area, but the value of 0.07 does not have a category. Given that 0.02 corresponds to a "barren or sparsely vegetated" area and 0.15 to a grassland, 0.07 was chosen to represent a transition area between the two (which is consistent with our choice that the center should represent a transition zone between a grassland and a barren area). The thermal inertia varies from 0.04 Cal cm^{-1}K^{-1}s$^{-0.5}$ in the edges of the computational domain to 0.025 Cal cm^{-1}K^{-1}s$^{-0.5}$ in its center. According to the CM1 documentation, the value of 0.04 Cal cm^{-1}K^{-1}s$^{-0.5}$ represents the thermal inertia of a forested area, 0.03 Cal cm^{-1}K^{-1}s$^{-0.5}$ corresponds to a grassland and 0.02 Cal cm^{-1}K^{-1}s$^{-0.5}$ corresponds to a "barren or sparsely vegetated" area. Given that the center of the domain is supposed to represent the transition between a grassland and a barren area, the value of 0.025 Cal cm^{-1}K^{-1}s$^{-0.5}$ is consistent with our choice. The albedo varies from 0.15 (forested area according to the CM1 documentation) to 0.22, which is between 0.19 (grassland according to the CM1 documentation) and 0.25 ("barren or sparsely vegetated" area according to the CM1 documentation). In addition to the modifications in the soil characteristics, the timestep used in the reference baroclinic jet run is 1 s. Using the same timestep as in the barotropic runs causes

15

instabilities to form early in the simulation. This simulation is not extended for as long as the reference Blackadar run because convection develops in the beginning of the fifth day and causes major disruptions in the flow.

The drier soil towards the center of the domain and consequent lack of evaporative cooling leads to the formation of a warm tongue similar to the one in figure 5 of S18 (figure 22). This warm tongue is periodic only because of the use of periodic boundaries, but there are large buffer zones between the baroclinic zones. Given the large extent of the domain compared to the region occupied by the buoyancy perturbation in the center, most of the boundary layer is unaffected by the circulations generated by the buoyancy maximum in the center. Therefore, a Blackdar type jet almost identical to the one in the Blackadar reference run develops in the area unaffected by the buoyancy gradient. However, in the areas with a buoyancy gradient, an additional pressure gradient force (related hydrostatically to the horizontal buoyancy gradient) is generated (apart from the initial one that creates the 10 m s^{-1} V wind), which creates additional circulations. To the right of the center of the warm tongue, the PFG generated by the buoyancy gradient enhances the background PGF, creating a much stronger southerly LLJ.

The strength of the LLJ that develops to the right of the center of the warm tongue increases with each passing day, reaching 18.60 m s^{-1} in the fifth day (figure 23), which is stronger than the reference Blackadar run. The LLJ peaks at 0130 LST, which is about two hours later than in the reference Blackadar jet run. The height of the maximum LLJ wind speed increases with each passing day, which could be related to the growth of the boundary layer height with each passing day. The structure of the jet in figure 23 is different from the reference Blackadar run (figure 4); there is a more defined peak at low levels instead of a uniform LLJ wind speed profile with height. What causes the more defined peak at low levels is the perturbation pressure gradient force created by the buoyancy gradient. The perturbation PGF is stronger at low levels, which creates a U wind profile that increases almost linearly with height within the lowest 3 kilometers (figure 24). Closer to the surface, friction slows down the U wind again, which creates a peak at low levels (otherwise the U wind would just keep decreasing all the way to the surface). The peak in the U also helps to generate a peak in the V wind profile through the Coriolis force (notice how the "Coriolis minus base PGF" curve in the bottom right panel of figure 24 shapes the V wind profile). As a result, there will also be a peak in the wind speed profile.

An ascent/descent zone similar to figure 6 of S18 develops in the center of the domain and the intensity of the ascent and descent phases increases during each day, as the buoyancy maximum in the center grows in intensity and the buoyancy gradient intensifies. Peak W velocities reach up to 3.6 cm s^{-1} and the maximum upward parcel displacement in a 24-hour period is 980 m for a parcel initially located 12 km to the west of the center of the warm tongue and 1426 m above the ground, which is consistent with the S18 theory. This parcel starts ascending in the fourth day of the simulation at 1130 LST (which is when the parcel starts being tracked) and stops ascending at 0430 LST of the fifth day of the simulation (which is when the

16

parcel stops being tracked). The ascent phase lasts around 16 hours, which is much longer than in S18. However, the S18 models only starts at sunset. After sunset, the ascent phase in this simulation lasts for about 8 hours while in S18 it lasts for approximately 7 hours.

The rising/sinking motion is associated with the convergence/divergence of the U wind in the center of the warm tongue; during the day, there is convergence in the center of the warm tongue since the perturbation PGF generated by the buoyancy gradient points towards its center (figure 25). However, turbulence (represented by the "PBL tendency term") acts against the perturbation PGF (notice how the "PBL tendency" curve in the bottom panels of figure 25 opposes the perturbation PGF) which results in an almost well-mixed U wind profile in both sides of the warm tongue. Turbulence mixes the winds in the boundary layer and therefore promotes the formation of a uniform profile (which would not happen if the perturbation PGF were allowed to act freely). The turbulence is capable of offsetting most of the effects of the perturbation PGF. However, it is incapable of creating a completely uniform wind profile, which results in the formation of weak ascent in the center of the domain for most of the afternoon. Once turbulence shuts down, the U wind profile rapidly starts evolving in accordance with the perturbation PGF and shifts into a configuration that is more convergent at low levels (figure 26), which is predicted by the S18 theory. Figure 26 corresponds to the time of maximum convergence (divergence) in the lower (upper) parts of the boundary layer (2230 LST) and also the time of peak vertical motion (also 2230 LST) in the fourth day of the simulation (figure 27). In the S18 model the peak rising motion occurs two and a half to three hours after sunset, while in this simulation the peak is two hours after sunset. Eventually, the rising motion gets replaced by the sinking motion (not shown) as the nocturnal oscillation of the LLJ winds evolves during the night. This occurs because the perturbation PGF remains mostly unaltered during the night, but the Coriolis force changes, which drives the nocturnal oscillation that starts with the shutdown of turbulence. In figure 27, the positive vertical motion is slightly shifted to the west because the average U wind is negative (large scale PGF points to the west).

The gravity wave response predicted by the S18 theory is present in this run in the form of the rising/sinking motion that develops in the center of the warm tongue in the boundary layer. The gravity waves originate in the center of the domain and can be seen as a series of descending phase fronts above the boundary layer (figure 28). They form as the air in the center of the positive vertical motion core hits the stably stratified free-atmosphere above the boundary layer.

In S18, the pattern of rising motion that develops in the center of the warm tongue descends with time and eventually gets replaced by sinking motion, which also happens in this run. Figure 29 shows the height of the maximum value of W in the lowest 4000 m of the domain for every hour. During the strongest part of the ascent phase in the warm tongue (from around 1730 LST to 0330 LST), the maximum vertical motion in the domain is located close to the center of the warm tongue. During this period (especially between 2030 LST of day 4 and 0030 LST of day 5) the vertical motion center descends with time, similar to what happens in S18.

17

The S16 analytical study has shown that a peak in the westerly winds occurs above the southerly jet and that this westerly jet descends with time during the night. A westerly jet has also been subsequently found in observational studies (Smith et al. 2019, Parsons et al. 2019). There is a maximum in the westerly winds (figure 30), but with a less well-defined jet than found, for example, in the S16 study. One possible explanation for this difference is that this simulation does not include sloping terrain.

b. Reference baroclinic jet run with modified initial geostrophic winds

Setting the free-atmosphere geostrophic wind to 0 m s^{-1} results in a weaker southerly LLJ in the eastern side of the warm tongue (figure 31) but a stronger maximum value of W (5.0 cm s^{-1}). In addition, the center of the vertical motion doesn't get advected to the west as in the reference baroclinic run. As a result, the ascent/descent zone sits above the buoyancy maximum in the center instead of slightly to the left of it, which likely explains why W is larger.

In an additional run, the free-atmosphere geostrophic wind was set to 15 m s^{-1}. This results in a stronger southerly LLJ in the eastern side of the warm tongue (not shown) and a weaker maximum value of W (2.0 cm s^{-1}). A weaker W most likely results from the ascent/descent zone being shifted more to the west than in the reference baroclinic run.

In the S18 theory, W does not depend on spatially constant free-atmosphere geostrophic winds. However, S18 does not retain the advection terms in the equations of motion, which means that the ascent area cannot be advected east or west.

c. Reference baroclinic jet run with modified Coriolis parameters

Two runs with Coriolis parameters of 7.72 × 10^{-5} s^{-1} and 1.028 × 10^{-4} s^{-1} corresponding to latitudes 30°N and 45°N were conducted. All other parameters were kept the same as in the reference baroclinic run, including the incoming solar radiation.

In the 30°N baroclinic run, the resulting LLJ is stronger than in the reference baroclinic run (20.80 m s^{-1}), which was expected, given that the same happened in the reference runs without baroclinicity. At 30°N, the LLJ peaks later than in the reference baroclinic run (around 0230 LST), which is consistent with a longer oscillation period at 30°N. The ascent phase in the center of the warm tongue lasts longer and is stronger (peak W values are larger), which could result from the fact that the Coriolis parameter is smaller. A smaller Coriolis parameter results in a longer inertial oscillation (larger inertial period), causing the convergent U wind pattern that forms after the shutdown of turbulence (same as figure 26) to last longer. A longer oscillation could translate into larger maximum values of W in the center if the length of the ascent phase is directly proportional to the intensity of W. The descending motion, however, appears to be around the same intensity as in the reference baroclinic run.

In the 45°N baroclinic run, the jet peaks slightly earlier than the reference baroclinic run (around 0030 LST), which is consistent with a shorter oscillation period at 45°N. The LLJ is also weaker than the baroclinic reference run (16.70 m s^{-1}), which was expected, since the same

happened in the reference runs without baroclinicity. The ascent phase in the center of the warm tongue lasts for a shorter period and is weaker (peak W values are smaller), which most likely results from the fact that the Coriolis parameter is smaller. A smaller Coriolis parameter results in a longer inertial oscillation, causing the convergent wind pattern that forms after the shutdown of turbulence (same as figure 26) to last for a shorter period of time. A shorter oscillation could translate into weaker maximum values of W in the center if the length of the ascent phase is directly proportional to the intensity of W. The descent phase is also weaker than in the reference baroclinic run. Because the period of both the ascent and descent phases is smaller, there is a secondary ascent phase (not shown) before the resumption of daytime turbulence has enough time to create a well-mixed boundary layer.

The LLJ peaks slightly earlier in the baroclinic (reference, 30°N and 45°N) runs than in the barotropic runs, but it's unclear why that happens.

d. Reference baroclinic jet run with modified warm tongue sizes

The DISTANCE parameters in equations (9), (10) and (11) were modified to 700 km/300 km to create a broader/narrower warm tongue in the center of the domain (which creates a decrease/increase in the buoyancy gradient). Increasing the DISTANCE parameter results in a weaker LLJ (maximum value of 17.24 m s^{-1}) and a weaker vertical motion in the ascent phase (maximum value of 2.0 cm s^{-1}). This was expected, given that the PGF created by the buoyancy gradient is weaker in a broader warm tongue. A reduction in the magnitude of the vertical motion in the ascent phase of a wave associated with a broader warm tongue also occurs in the S18 model. Increasing the DISTANCE parameter increases the width of the positive vertical motion area during the ascent phase when compared to the reference baroclinic run.

Decreasing the DISTANCE parameter results in a stronger LLJ (maximum value of 21.60 m s^{-1}) and also a stronger maximum vertical motion in the ascent phase (7.3 cm s^{-1}). This was expected, given that the PGF created by the buoyancy gradient is stronger in a narrower warm tongue. An increase in the magnitude of the vertical motion in the ascent phase of a wave associated with a narrower warm tongue also occurs in the S18 model. Decreasing the DISTANCE parameter decreases the width of the positive vertical motion area during the ascent phase when compared to the reference baroclinic run. Maximum upward parcel displacement in a 24-hour period is 1600 m for a parcel initially located 28 km to the west of the center of the warm tongue and 868 m above the ground. This parcel starts ascending in the fourth day of the simulation at 1230 LST (which is when it starts being tracked) and stops ascending at 0330 LST of the fifth day of the simulation (which is when it stops being tracked).

The width of the baroclinic zone when the DISTANCE parameter is set to 300 km is about the same as when the wavelength of the initial thermal perturbations (λ) is set to 1000 km in the S18 model. Using λ = 1000 km, a free-atmosphere Brunt–Väisälä frequency (N) of 0.01 and f = 0.000086, S18 was able to obtain a maximum ascent of 5.0 cm s^{-1} with an ascent phase lasting 7 hours and upward maximum parcel displacements of up 750 m. In this simulation, N is

approximately 0.007 in the free atmosphere and f = 0.000084. The resulting maximum ascent is 7.3 cm s^{-1}, the maximum upward parcel displacement is 1600 m, and the duration of the ascent phase is 14 hours (starting around noon), all of which have a higher magnitude than in S18. However, the buoyancy gradient (approximately 1.68 $\times$ 10^{-3} m s^{-2} km^{-1} compared to 2.0 $\times$ 10^{-3} m s^{-2} km^{-1} in S18) and potential temperature gradient (0.01 K km^{-1} compared with 0.016 K km^{-1} in S18) are smaller than in the S18 model.

In the S18 analytical model, it was found that the duration of the low-level ascent increased as the wavelength of the thermal perturbation increased. This did not occur in the simulations with broader and narrower warm tongues.

e. Reference baroclinic jet run with hill shaped terrain

This run is similar to the reference baroclinic run, but the baroclinicity arises from the presence of terrain instead of a gradient in surface layer moisture. There are no lateral variations in moisture, albedo and thermal inertia, and the surface characteristics are the same as in the reference Blackadar jet run. The terrain height is defined as:

$$\text{HEIGHT} = \text{MAXHEIGHT} \times \exp\left(-x^2/_{\text{DISTANCE}^2}\right) \tag{12},$$

where MAXHEIGHT is the maximum height of the terrain (1 km), x is the distance to the center of the domain (negative to the left of the center of the domain and positive to the right) and DISTANCE is the e folding distance (set to 500 km). The result is a hill of 1 km in height that peaks in the center of the domain. As in the reference baroclinic jet run, the effects of the circulation induced by the terrain do not affect most of the domain, where barotropic LLJs almost identical to the ones in the reference Blackadar run develop. This simulation is not extended for as long as the reference baroclinic and Blackadar jet runs because convection develops in the middle of the fourth day and causes major disruptions in the flow.

The structure of the LLJ that develops to the right of center of the domain is very similar to the LLJ that develops to the right of the warm tongue in the reference baroclinic run (figure 32). The LLJ peaks around 0130 LST, which is the same as in the reference baroclinic run. However, it is stronger than the reference baroclinic run (maximum value of 20.20 m s^{-1}). Because convection develops in the fourth day of the simulation, the maximum value of 20.20 m s^{-1} applies to the third LLJ that develops in this simulation, while in the reference baroclinic run, the maximum value of wind speed is found in the fourth jet (one day later). Similar to the baroclinic jet run, the height of the maximum winds in the LLJ increases every day.

Adding terrain creates a vertical motion pattern that is very similar to the one that develops in the reference baroclinic run (not shown). The ascent and descent phases last the same amount of time and the peak positive and negative vertical motion occur at the same time (and also descend with time). However, the positive vertical motion in the center of the domain during the ascent phase is stronger (maximum value of 5.2 cm s^{-1}). The maximum W of 5.2 cm s^{-1} occurs in the third day of the simulation, while in the baroclinic jet run it occurs in the fourth. Given that the vertical motion increases with each passing day in this simulation, the difference

in the maximum value of W in the reference baroclinic run and this run would be larger if convection didn't form in the fourth day of this simulation. The structure of thermal perturbation in the center is also very similar, but its magnitude is larger (figure 33). As in the reference baroclinic run, the center of the thermal perturbation is slightly advected to the west of the center of the domain. The gravity waves that formed in the center of the domain as the air in the center of the positive vertical motion core hits the stably stratified free-atmosphere in the reference baroclinic run are also present in this simulation.

f. Reference baroclinic jet run with hill shaped terrain and soil moisture gradient

This simulation is exactly the same as the reference baroclinic run but with the inclusion of a hill shaped terrain as was done in the reference baroclinic run with hill shaped terrain. The resulting flow behaves qualitatively the same as the refence baroclinic run and the reference baroclinic run with hill shaped terrain, but key parameters discussed for those two runs are magnified: the maximum speed of the LLJ in the right side of the terrain is 25.80 m s^{-1} and the maximum value of vertical motion is 17.0 cm s^{-1}.

5. Summary and Conclusions

The CM1 model was used to simulate LLJs under different scenarios. The LLJ simulated in barotropic conditions (reference Blackadar jet) is nearly uniform with height in most of the boundary layer instead of having a defined peak at low levels. This LLJ peaks slightly earlier than jets observed in the Great Plains (Buajitti and Blackadar 1957, Mitchell et al. 1995, Arritt et al. 1997, Whiteman et al. 1997), possibly because the turbulence shuts down earlier in the simulations than in reality. It was found that the strength of the LLJ decays with time as the height of the boundary layer grows, except in the reference Blackadar run at 30°N. LLJs also were stronger in the simulations with shallower boundary layers. It is possible that the turbulent mixing is stronger in shallower boundary layers, which results in a larger ageostrophic wind and stronger LLJs. Increasing the value of the roughness elements also results in stronger LLJs. Changing the Coriolis parameter to represent a location at 30°N/45°N resulted in stronger/weaker barotropic LLJs. Stronger/weaker jets at 30°N/45°N are consistent with the Du and Rotunno (2014) analytical model and with the Shibuya et al. (2014) idea of a resonance-like amplification of the inertial oscillation which is largest at 30°N.

The LLJ simulated in baroclinic conditions (reference baroclinic jet run) was stronger than in barotropic conditions, which also occurs in the S16 model and in the S22 model when baroclinicity is added (trough the introduction of a slope in the S16 model and through the introduction of a surface buoyancy gradient in S22). Ascent and descent phases were observed in the center of the baroclinic zone (warm tongue) resulting in upward parcel displacements that could facilitate convection initiation. Ascent phases last about 16 hours and the maximum parcel displacement was 980 m. Changing the Coriolis parameter to represent a location at

21

30°N/45°N resulted in an increase/decrease in LLJ strength and in the magnitude of the positive vertical motion in the ascent phase and also caused the ascent phase to last for a longer/shorter period of time. Increasing/decreasing the value of the free-atmosphere geostrophic wind resulted in stronger/weaker LLJs and a decrease/increase in the magnitude of the positive vertical motion in the ascent phase. Increasing/decreasing the width of the warm tongue resulted in a decrease/increase in the LLJ strength and in the magnitude of the positive vertical motion in the ascent phase and also resulted in a wider/narrower ascent zone. The height of the peak W in the baroclinic jets increases with time, which is likely a result of the growth of the boundary layer with each passing day. Unlike the barotropic LLJs, the baroclinic LLJs had a defined peak at low levels due to the perturbation PGF associated with the buoyancy gradient.

The long duration of the ascent with a peak found later in the night in the baroclinic simulations suggest possible relevance of the S18 mechanism to support the occurrence of nocturnal convection. However, numerous studies beginning with Parsons et al. (1991) have revealed that far stronger (m s^{-1}) ascent can occur on the Great Plains slope during late afternoon and early evening in association with sharp temperature differences that occur in association with the dryline that frequently occurs over this region. The concept of an in-land sea breeze first described by Sun and Ogura (1979) suggests an association between the thermal gradients on the sloping terrain, the dryline, and the LLJ. Thus, while our results do support nocturnal ascent, some caution should be considered when applying these results to the nocturnal environment over the Great Plains as the simulations do not include a realistic sloping terrain, vertical shear and gradients in water vapor and cloud cover. These characteristics are often found in the LLJ environment over the Great Plains.

Most of the features in S18 are present in the baroclinic simulations; the formation of a wave characterized by ascent and descent phases in the center of the warm tongue, peak vertical motion occurring after sunset and a descending vertical motion center. Specifically, S18 predicted that the peak vertical motion would occur after sunset because of the shutdown of turbulence, which the analytical model oversimplified as an instantaneous process. However, it is possible to verify the gross aspects of this analytical prediction using numerical simulations, as was done in this study, which has shown that the shutdown of daytime turbulence (figures 25 and 26) enables the formation of a circulation more conducive to convergence which leads to the peak W values in the ascent phase occurring after sunset. However, some features in the S18 model were not present in this study. In the S18 model, the ascent phase lasts for a longer/shorter period of time when the width of the baroclinic zone increases/decreases, which does not occur in this study. The sensitivity of W in the ascent area to a spatially constant free-atmosphere geostrophic wind does not occur in the S18 model.

This study attempts to create an environment more realistic than the one in S18 and test if the main predictions of the S18 theory still hold true in this new environment. Although the numerical setting used in this study is able to reproduce more faithfully the Great Plains environment than the S18 model, there are still some major features that could not be reproduced, such as a non-uniform free-atmosphere geostrophic wind and a realistic

atmospheric moisture profile. The lack of atmospheric moisture in the simulations compared with the Great Plains environment is arguably the most important difference between the numerical setting in this study and the real atmosphere. Due to the lack of atmospheric moisture, the inversion that forms during nighttime in both the center and the edges of the computational domain is too shallow, which contributes to the formation of the shallow peak in the U wind profile seen in figure 7. One possible solution to this issue is to modify the microphysics scheme in order to prevent cloud formation even if the relative humidity crosses 100%. Cloud formation and convection are currently the biggest issues we are facing, and it is the reason why most of the simulations cannot be extended for more than 5 days. Apart from modifying the microphysics scheme, we are looking into other ways of delaying the formation of clouds, such as experimenting with other boundary layer schemes and using different numerical models.

Given that the numerical setting in this study is very idealized and relatively simple, the results of this study are not necessarily applicable to the Great Plains. In order to increase the complexity of the simulated environment, available options are to conduct the same simulations using large eddy simulations or use the Weather Research and Forecasting (WRF) model to look at real cases of warm tongues/LLJs in the Great Plains. The geostrophic wind can be changed to more realistic values instead of being uniform with height. Another possibility is to use reanalysis data to check for the presence of low-level ascent/LLJs associated with warm tongues in the Great Plains. However, given that most of what was predicted by S18 occurred in the baroclinic simulations, we feel more confident that the same processes are occurring in the real atmosphere.

REFERENCES:

Arritt, R. W., T. D. Rink, M. Segal, D. P. Todey, C. A. Clark, M. J. Mitchell, and K. M. Labas, 1997: The Great Plains low-level jet during the warm season of 1993. *Mon. Wea. Rev.*, **125**, 2176–2192, https://doi.org/10.1175/1520-0493(1997)125<2176:TGPLLJ>2.0.CO;2.

Baas, P., F. C. Bosveld, H. Klein Baltink, and A. A. M. Holtslag, 2009: A climatology of nocturnal low-level jets at Cabauw. *J. Appl. Meteor. Climatol.*, **48**, 1627–1642, https://doi.org/10.1175/ 2009JAMC1965.1.

Beebe, R. G., and F. C. Bates, 1955: A mechanism for assisting in the release of convective instability. *Mon. Wea. Rev.,* **83,** 1–10, https://doi.org/10.1175/1520-0493(1955)083<3C0001:AMFAIT>3E2.0.CO;2.

Blackadar, A. K., 1957: Boundary layer wind maxima and their significance for the growth of nocturnal inversions. *Bull. Amer. Meteor. Soc.*, **38**, 283–290, https://doi.org/10.1175/1520-0477-38.5.283.

Blake, B. T., D. B. Parsons, K. R. Haghi, and S. G. Castleberry, 2017: The structure, evolution, and dynamics of a nocturnal convective system simulated using the WRF-ARW Model. *Mon. Wea. Rev.*, **145**, 3179–3201, https://doi.org/10.1175/ MWR-D-16-0360.1.

Bonner, W. D., 1966: Case study of thunderstorm activity relation to the low-level jet. *Mon. Wea. Rev.,* **94,** 167–178, https://doi.org/10.1175/1520-0493(1966)094<3C0167:CSOTAI>3E2.3.CO;2.

Bonner, W. D., 1968: Climatology of the low level jet. *Mon. Wea. Rev.*, **96**, 833–850, https://doi.org/10.1175/1520-0493(1968)096<0833:COTLLJ>2.0.CO;2.

Bonner, W. D., and J. Paegle, 1970: Diurnal variations in boundary layer winds over the south-central United States in summer. *Mon. Wea. Rev.*, **98**, 735–744, https://doi.org/10.1175/1520-0493(1970)098<0735:DVIBLW>2.3.CO;2.

Bryan, G. H., and J. M. Fritsch, 2002: A benchmark simulation for moist nonhydrostatic numerical models. *Mon. Wea. Rev.*, **130**, 2917–2928, https://doi.org/10.1175/1520-0493(2002)130<3C2917:ABSFMN>3E2.0.CO;2.

Bryan, G. H., and R. Rotunno, 2009: The maximum intensity of tropical cyclones in axisymmetry numerical model simulations. *Mon. Wea. Rev.*, **137**, 1770–1789, https://doi.org/10.1175/2008MWR2709.1.

Buajitti, K., and A. K. Blackadar, 1957: Theoretical studies of diurnal wind-structure variations in the planetary boundary layer. *Quart. J. Roy. Meteor. Soc.*, **83**, 486–500, https://doi.org/10.1002/qj.49708335804.

Carbone, R. E., and J. D. Tuttle, 2008: Rainfall occurrence in the U.S. warm season: The diurnal cycle. *J. Climate*, **21**, 4132–4146, https://doi.org/10.1175/2008JCLI2275.1.

Dai, A., F. Giorgi, and K. E. Trenberth, 1999: Observed and model-simulated diurnal cycles of precipitation over the contiguous United States. *J. Geophys. Res.*, **104**, 6377–6402, https://doi.org/10.1029/98JD02720.

Davis, C. A., K. W. Manning, R. E. Carbone, S. B. Trier, and J. D. Tuttle, 2003: Coherence of warm-season continental rainfall in numerical weather prediction models. *Mon. Wea. Rev.*, **131**, 2667–2679, https://doi.org/10.1175/1520-0493(2003)131<2667:COWCRI>2.0.CO;2.

Du, Y., and R. Rotunno, 2014: A simple analytical model of the nocturnal low-level jet over the Great Plains of the United States. *J. Atmos. Sci.*, **71**, 3674–3683, doi:10.1175/JAS-D-14-0060.1.

Fiedler, S., K. Schepanski, B. Heinold, P. Knippertz, and I. Tegen, 2013: Climatology of nocturnal low-level jets over North Africa and implications for modeling mineral dust emission. *J. Geophys. Res. Atmos.*, **118**, 6100–6121, https://doi.org/10.1002/jgrd.50394.

Gebauer, J. G., A. Shapiro, E. Fedorovich, and P. Klein, 2018: Convection initiation caused by heterogeneous low-level jets over the Great Plains. *Mon. Wea. Rev.*, **146**, 2615–2637, https://doi.org/ 10.1175/MWR-D-18-0002.1.

Gebauer, J. G., and A. Shapiro, 2019: Clarifying the baroclinic contribution to the Great Plains low-level jet frequency maximum. *Mon. Wea. Rev.*, **147**, 3481–3493, https://doi.org/10.1175/MWR-D-19-0024.1.

Holton, J. R., 1967: The diurnal boundary layer wind oscillation over sloping terrain. *Tellus*, **19A**, 199–205, https://doi.org/10.1111/j.2153-3490.1967.tb01473.x.

Hong, S.-Y. and H.-L. Pan, 1996: Nonlocal boundary layer vertical diffusion in a medium-range forecast model. *Mon. Wea. Rev.*, **124**, 2322–2339.

Hong, S.-Y., Y. Noh, and J. Dudhia, 2006: A new vertical diffusion package with an explicit treatment of entrainment processes. *Mon. Wea. Rev.*, **134**, 2318–2341, https://doi.org/10.1175/MWR3199.1.

Hoskins, B. J., M. E. McIntyre, and A. W. Robertson, 1985: On the use and significance of isentropic potential vorticity maps. *Quart. J. Roy. Meteor. Soc.*, **111**, 877–946, https://doi.org/ 10.1002/qj.49711147002.

Jiang, X., N. C. Lau, I. M. Held, and J. J. Ploshay, 2007: Mechanisms of the Great Plains low-level jet as simulated in an AGCM. *J. Atmos. Sci.*, **64**, 532–547, https://doi.org/10.1175/ JAS3847.1.

Jiménez, P. A., J. Dudhia, J. F. González-Rouco, J. Navarro, J. P. Montávez, and E. García-Bustamante, 2012: A revised scheme for the WRF surface layer formulation. *Mon. Wea. Rev.*, **140**, 898–918, https://doi.org/10.1175/MWR-D-11-00056.1.

Jirak, I. L., and W. R. Cotton, 2007: Observational analysis of the predictability of mesoscale convective systems. *Wea. Forecasting*, **22**, 813–838, https://doi.org/10.1175/WAF1012.1.

Klein, P. M., X.-M. Hu, A. Shapiro, and M. Xue, 2016: Linkages between boundary-layer structure and the development of nocturnal low-level jets in central Oklahoma. *Bound.-Layer Meteor.*, **158**, 383–408, https://doi.org/10.1007/s10546-015-0097-6.

Knievel, J., G. Bryan, and J. Hacker, 2007: Explicit numerical diffusion in the WRF model. *Mon. Wea. Rev.*, **135**, 3808–3824, https://doi.org/10.1175/2007MWR2100.1.

Kumar, V., J. Kleissl, C. Meneveau, and M. B. Parlange, 2006: Large-eddy simulation of a diurnal cycle of the atmospheric boundary layer: Atmospheric stability and scaling issues. *Water Resour. Res.*, **42**, W06D09, doi:10.1029/2005WR004651.

Lee, M.-I., S. D. Schubert, M. J. Suarez, J.-K. E. Schemm, H.-L.Pan, J. Han, and S.-Y. Yoo, 2008: Role of convection triggers in the simulation of the diurnal cycle of precipitation over the United States Great Plains in a general circulation model. *J. Geophys. Res.*, **113**, D02111, https://doi.org/10.1029/2007JD008984.

Li, Y., and R. B. Smith, 2010: The detection and significance of diurnal pressure and potential vorticity anomalies east of the Rockies. *J. Atmos. Sci.*, **67**, 2734–2751, https://doi.org/10.1175/ 2010JAS3423.1.

Maddox, R. A., C. F. Chappell, and L. R. Hoxit, 1979: Synoptic and meso-α scale aspects of flash flood events. *Bull. Amer. Meteor. Soc.*, **60**, 115–123, https://doi.org/10.1175/1520-0477- 60.2.115.

Marengo, J. A., W. R. Soares, C. Saulo, and M. Nicolini, 2004: Climatology of the low-level jet east of the Andes as derived from the NCEP–NCAR reanalyses: Characteristics and temporal variability. *J. Climate,* **17,** 2261–2280, https://doi.org/10.1175/15200442(2004)017<3C2261:COTLJE>3E2.0.CO;2.

Mitchell, M. J., R. W. Arritt, and K. Labas, 1995: A climatology of the warm season Great Plains low-level jet using wind profiler observations. *Wea. Forecasting*, *10*, 576–591, https://doi.org/10.1175/ 1520-0434(1995)010<0576:ACOTWS>2.0.CO;2.

Parish, T. R., and L. D. Oolman, 2010: On the role of sloping terrain in the forcing of the Great Plains low-level jet. *J. Atmos. Sci.*, **67**, 2690–2699, https://doi.org/10.1175/2010JAS3368.1.

Parsons, D., K. Haghi, K. Halbert, B. Elmer, and J. Wang, 2019: The potential role of atmospheric bores and gravity waves in the initiation and maintenance of nocturnal convection over the Southern Great Plains. *J. Atmos. Sci.*, **76**, 43–68, https://doi.org/10.1175/JAS-D-17-0172.1.

Parsons, D. B., M. A. Shapiro, R. M. Hardesty, R. J. Zamora, and J.M. Intrieri, 1991: The fine-scale structure of a west Texas dry-line. *Mon. Wea. Rev.*, **119**, 1242–1258.

Pham, N. T., K. Nakamura, F. A. Furuzawa, and S. Satoh, 2008: Characteristics of low level jets over Okinawa in the Baiu and post-Baiu seasons revealed by wind profiler observations. *J. Meteor. Soc. Japan*, **86**, 699–717, https://doi.org/10.2151/jmsj.86.699.

Pu, B., and R. E. Dickinson, 2014: Diurnal spatial variability of Great Plains summer precipitation related to the dynamics of the low-level jet. *J. Atmos. Sci.*, **71**, 1807–1817, https://doi.org/10.1175/JAS-D-13-0243.1.

Raymond, D. J., and H. Jiang, 1990: A theory for long-lived mesoscale convective systems. *J. Atmos. Sci.*, **47**, 3067–3077.

Reif, D. W., and H. B. Bluestein, 2017: A 20-year climatology of nocturnal convection initiation over the central and southern Great Plains during the warm season. *Mon. Wea. Rev.*, **145**, 1615–1639, https://doi.org/10.1175/MWR-D-16-0340.1.

Reif, D. W., and H. B. Bluestein, 2018: Initiation mechanisms of nocturnal convection without nearby surface boundaries over the central and southern Great Plains during the warm season. *Mon. Wea. Rev.*, **146**, 3053–3070, https://doi.org/10.1175/MWR-D-18-0040.1.

Salio, P., M. Nicolini, and C. Saulo, 2002: Chaco low-level jet events characterization during the austral summer season. *J. Geophys. Res.,* **107,** 4816, https://doi.org/10.1029/2001JD001315.

Shapiro, A., and E. Fedorovich, 2009: Nocturnal low-level jet over a shallow slope. *Acta Geophys.*, **57**, 950–980, https://doi.org/10.2478/s11600-009-0026-5.

Shapiro, A., E. Fedorovich, and S. Rahimi, 2016: A unified theory for the Great Plains nocturnal low-level jet. *J. Atmos. Sci.*, **73**, 3037–3057, https://doi.org/10.1175/JAS-D-15-0307.1.

Shapiro, A., E. Fedorovich, and J. B. Gebauer, 2018: Mesoscale ascent in nocturnal low-level jets. *J. Atmos. Sci.*, **75**, 1403–1427, https://doi.org/10.1175/JAS-D-17-0279.1.

Shapiro, A., Gebauer, J. G., and D. B. Parsons, 2022: Emergence of a nocturnal low-level jet from a broad baroclinic zone. *J. Atmos. Sci.* (in press).

Shibuya, R., K. Sato, and M. Nakanishi, 2014: Diurnal wind cycles forcing inertial oscillations: A latitude-dependent resonance phenomenon. *J. Atmos. Sci.*, **71**, 767–781, doi:10.1175/JAS-D-13-0124.1.

Smith, E. N., J. G. Gebauer, P. M. Klein, E. Fedorovich, and J. A. Gibbs, 2019: The Great Plains low-level jet during PECAN: Observed and simulated characteristics. *Mon. Wea. Rev.*, **147**, 1845–1869, https://doi.org/10.1175/MWR-D-18-0293.1.

Song, J., K. Liao, R. L. Coulter, and B. M. Lesht, 2005: Climatology of the low-level jet at the Southern Great Plains Atmospheric Boundary Layer Experiments site. *J. Appl. Meteor.*, **44**, 1593–1606, https://doi.org/10.1175/JAM2294.1.

Song, H., W. Lin, Y. Lin, A. Wolf, R. Neggers, L. J. Donner, A. D. Del Genio, and Y. Liu, 2013: Evaluation of precipitation simulated by seven SCMs against the ARM observations at the SGP site. *J. Climate*, **26**, 5467–5492, https://doi.org/10.1175/ JCLI-D-12-00263.1.

Storm, B., J. Dudhia, S. Basu, A. Swift, and I. Giammanco, 2009: Evaluation of the Weather Research and Forecasting model on forecasting low-level jets: Implications for wind energy. *Wind Energy*, **12**, 81–90, https://doi.org/10.1002/we.288.

Sun, W.-Y., and Y. Ogura, 1979: Boundary-layer forcing as a possible trigger to squall-line formation. *J. Atmos. Sci.*, **36**, 235–254, https://doi.org/10.1175/1520-0469(1979)036<0235:BLFAAP>2.0.CO;2.

Tang, S., Gleckler, P., Xie, S., Lee, J., Ahn, M. S., Covey, C., & Zhang, C. (2021). Evaluating the diurnal and semidiurnal cycle of precipitation in CMIP6 models using satellite and ground-based observations. *Journal of Climate*, *34*(8), 3189–3210. https://doi.org/10.1175/ JCLI-D-20-0639.1.

Trier, S. B., and D. B. Parsons, 1993: Evolution of environmental conditions preceding the development of a nocturnal mesoscale convective complex. *Mon. Wea. Rev.*, **121**, 1078–1098, https://doi.org/10.1175/1520-0493(1993)121<1078:EOECPT>2.0.CO;2.

Tuttle, J. D., and C. A. Davis, 2006: Corridors of warm season precipitation in the central United States. *Mon. Wea. Rev.*, **134**, 2297–2317, https://doi.org/10.1175/MWR3188.1.

Wallace, J. M., 1975: Diurnal variations in precipitation and thunderstorm frequency over the conterminous United States. *Mon. Wea. Rev.*, **103**, 406–419, https://doi.org/10.1175/1520-0493(1975)103<0406:DVIPAT>2.0.CO;2.

Walters, C. K., and J. A. Winkler, 2001: Airflow configurations of warm season southerly low-level wind maxima in the Great Plains. Part I: Spatial and temporal characteristics and relationship to convection. *Wea. Forecasting*, **16**, 513–530, https://doi.org/10.1175/1520-0434(2001)016<0513:ACOWSS>2.0.CO;2.

——, ——, S. Husseini, R. Keeling, J. Nikolic, and S. Zhong, 2014: Low-level jets in the North American Regional Reanalysis (NARR): A comparison with rawinsonde observations. *J. Appl. Meteor. Climatol.*, **53**, 2093–2113, https://doi.org/10.1175/JAMC-D-13-0364.1.

Weckwerth, T. M., and Coauthors, 2004: An overview of the International H2O Project (IHOP_2002) and some preliminary highlights. *Bull. Amer. Meteor. Soc.*, **85**, 253–277, https://doi.org/10.1175/BAMS-85-2-253.

Whiteman, C. D., X. Bian, and S. Zhong, 1997: Low-level jet climatology from enhanced rawinsonde observations at a site in the southern Great Plains. *J. Appl. Meteor.*, **36**, 1363–1376, https://doi.org/10.1175/1520-0450(1997)036<1363:LLJCFE>2.0.CO;2.

Wilson, J. W., and R. D. Roberts, 2006: Summary of convective storm initiation and evolution during IHOP: Observational and modeling perspective. *Mon. Wea. Rev.*, **134**, 23–47, https://doi.org/10.1175/MWR3069.1.
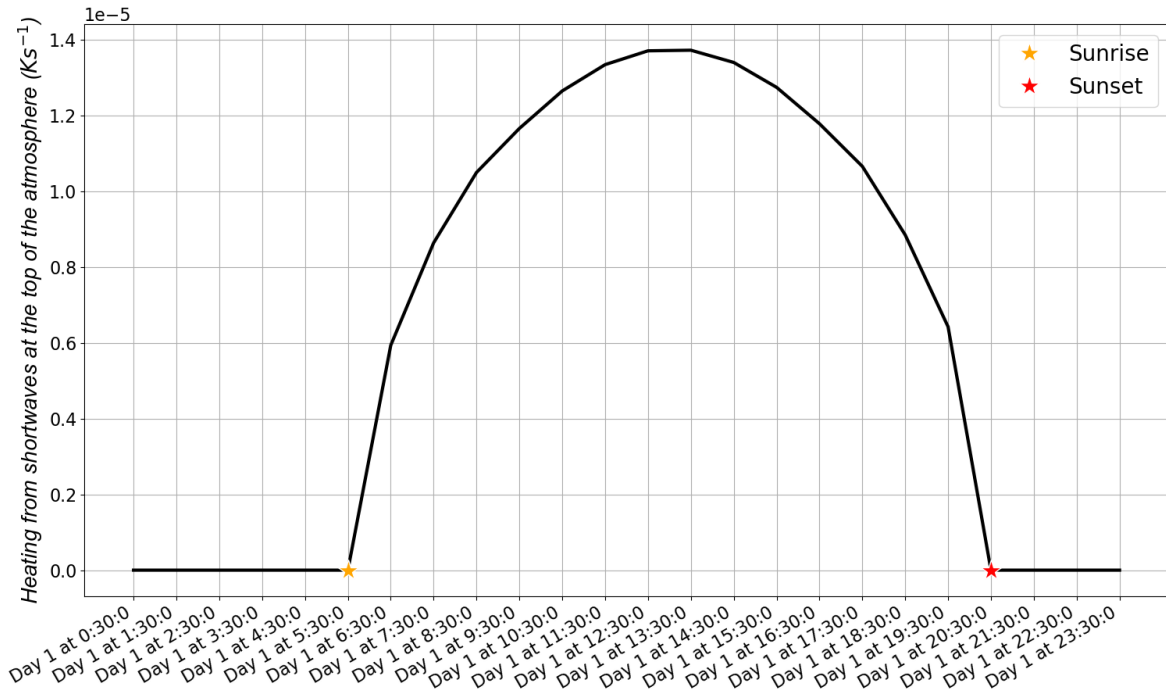
FIGURES:

Figure 1. Heating from shortwaves in the top of the atmosphere in the first day of the simulations (all days look the same).
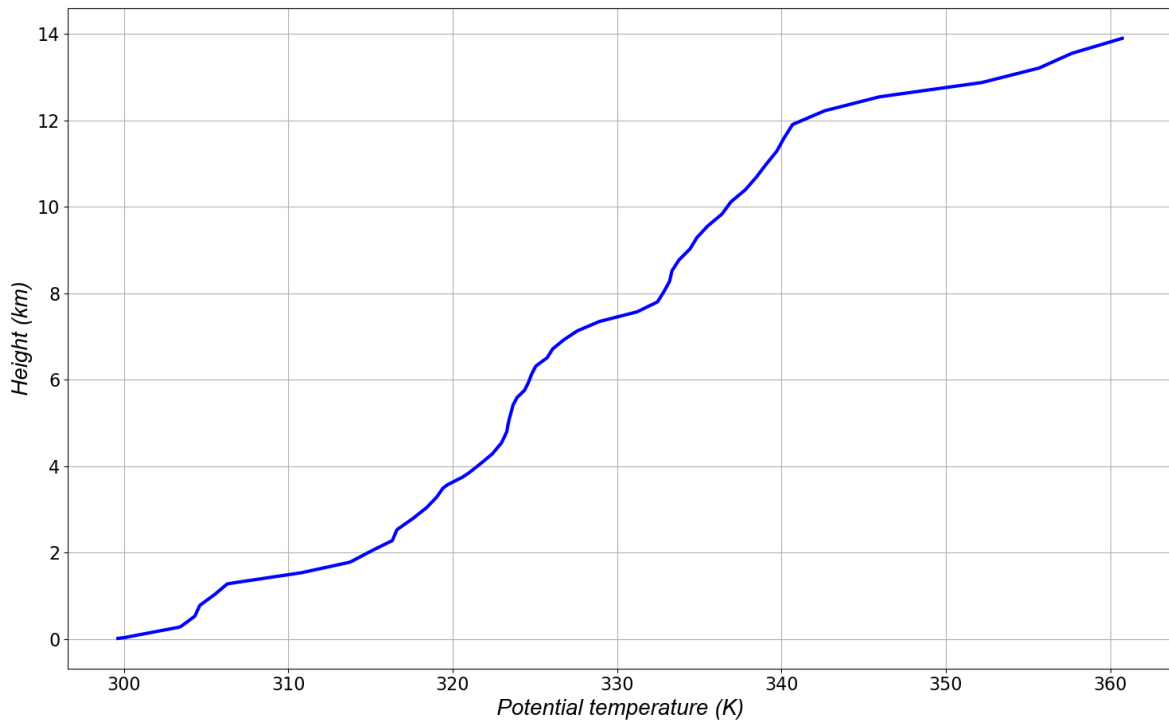
Figure 2. Initial potential temperature profile.
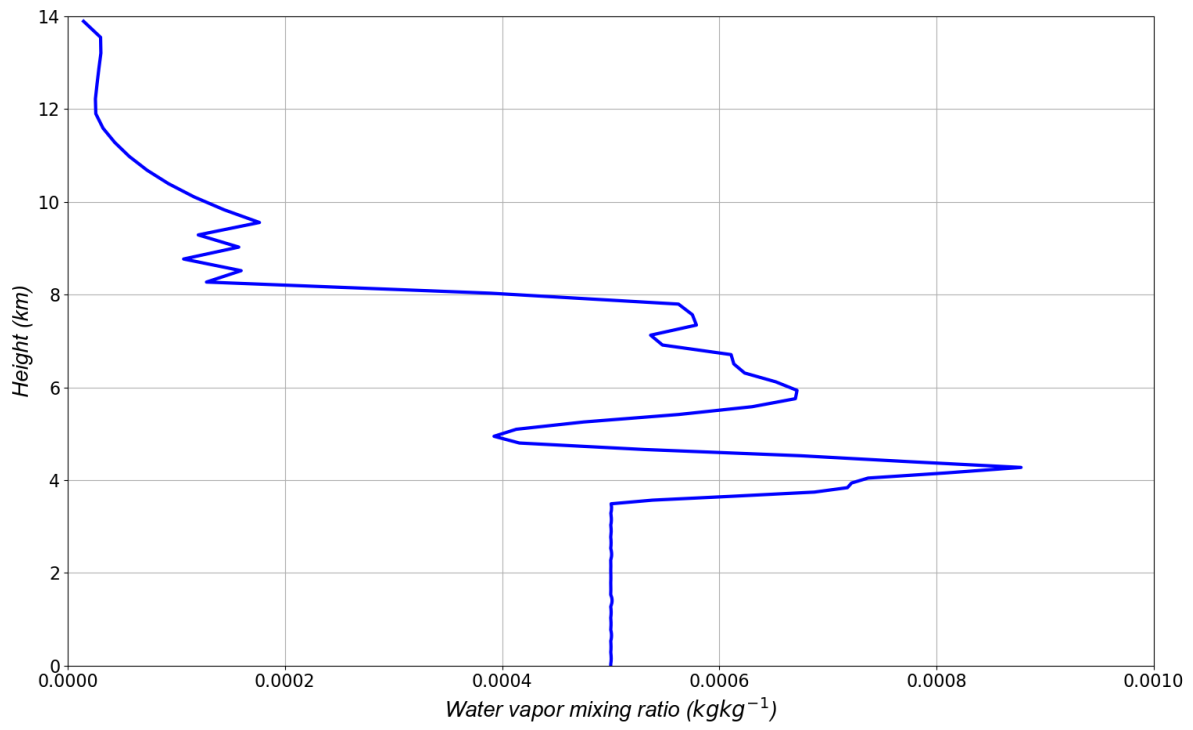
Figure 3. Moisture profile used to initialize the simulations.
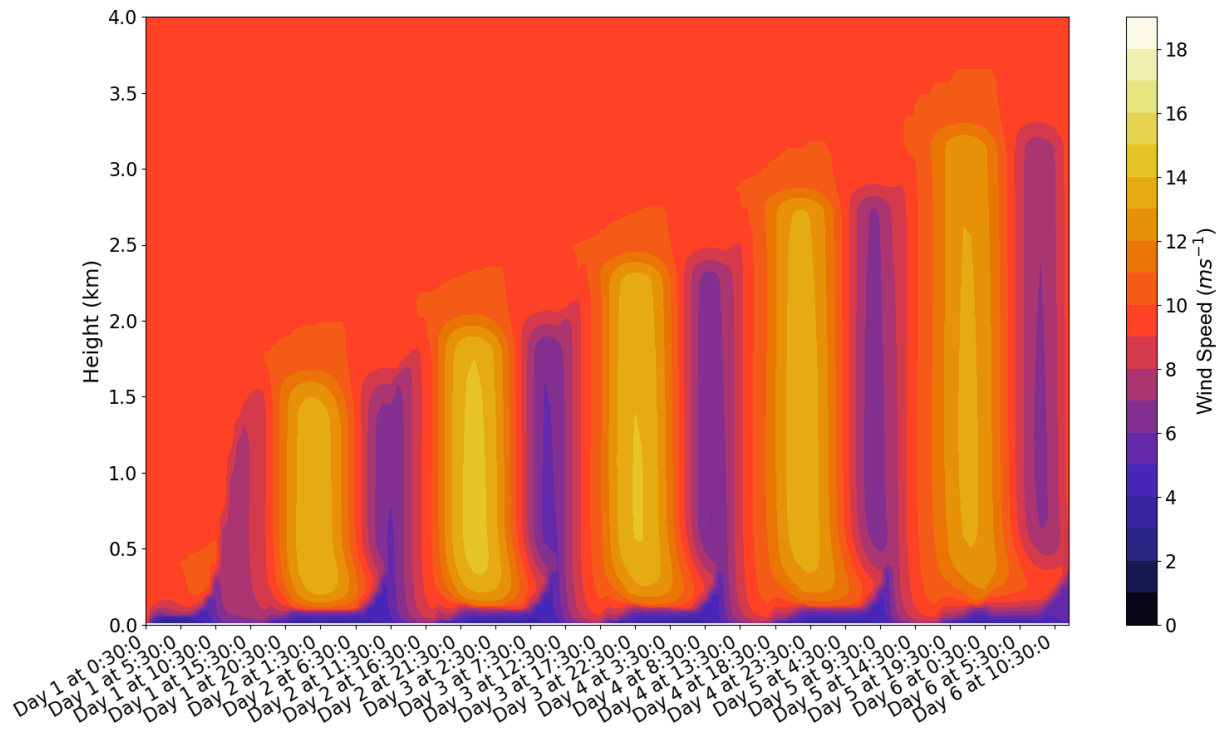
Figure 4. Wind speed as a function of time and height for the reference Blackadar run.
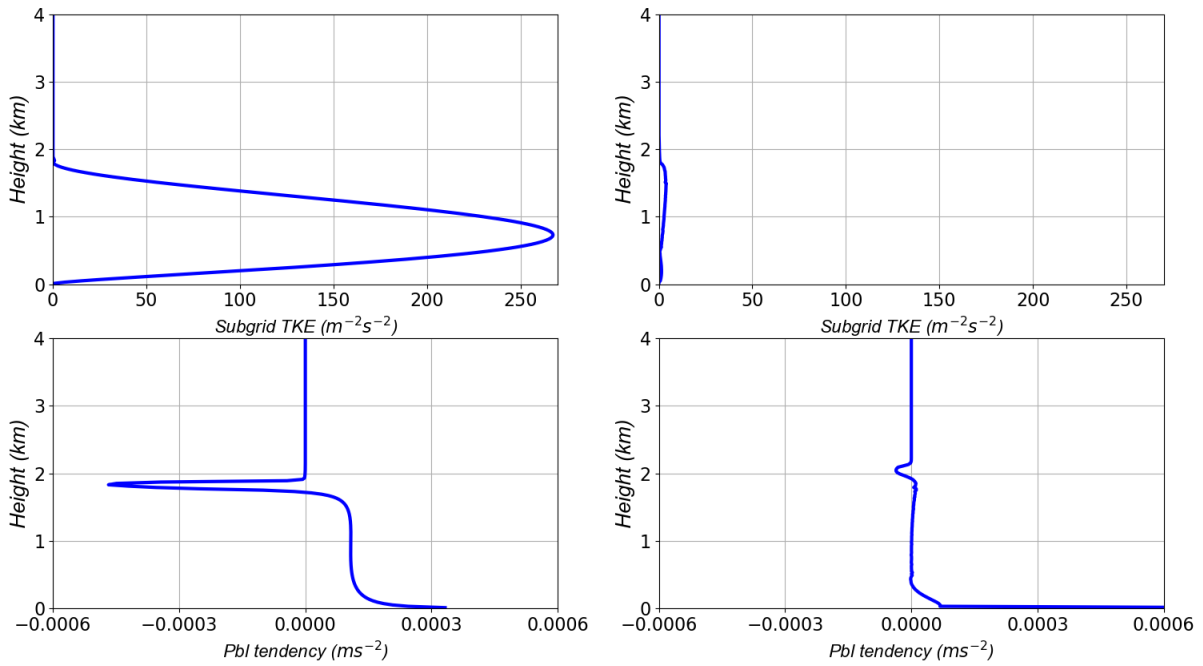
Figure 5. Subgrid TKE at 0230 LST of the second day of the simulation (top left panel), subgrid TKE at 1930 LST of the second day of the simulation (top right panel), "PBL tendency" at 0230 LST of the second day of the simulation (bottom left panel) and "PBL tendency" at 1930 LST of the second day of the simulation (bottom right panel). In this figure, the "PBL tendency" only applies to the U wind field.
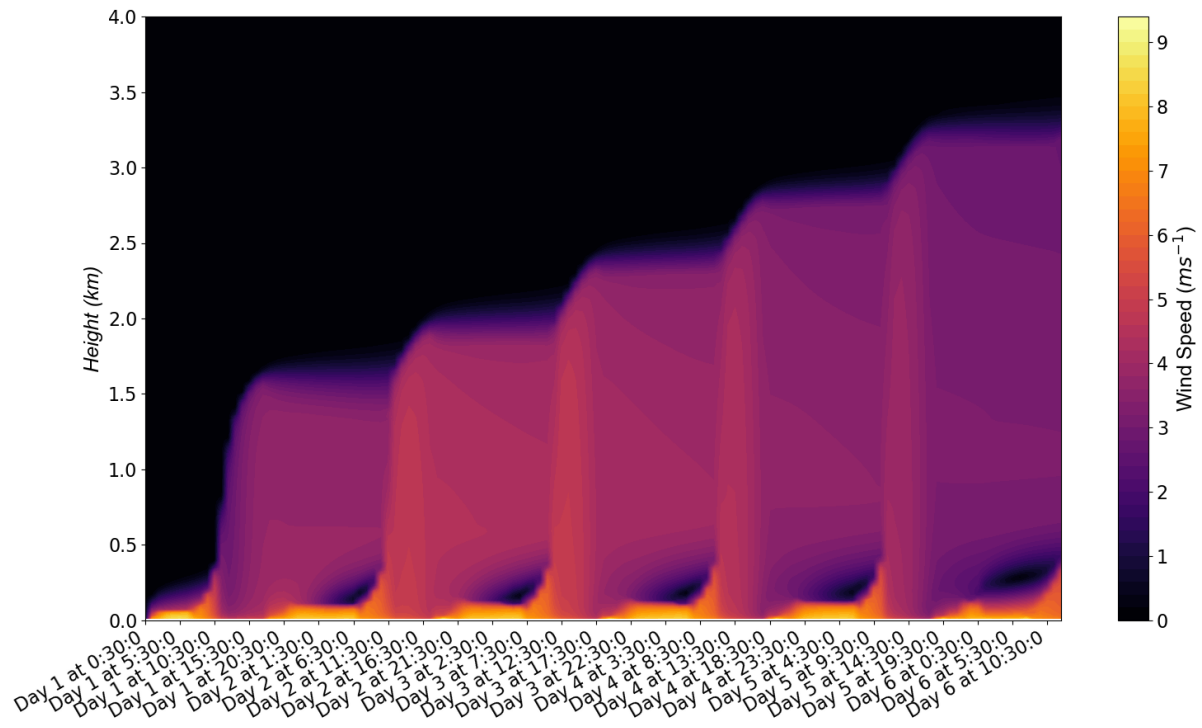
Figure 6. Ageostrophic wind speed as a function of time and height for the reference Blackdar run.
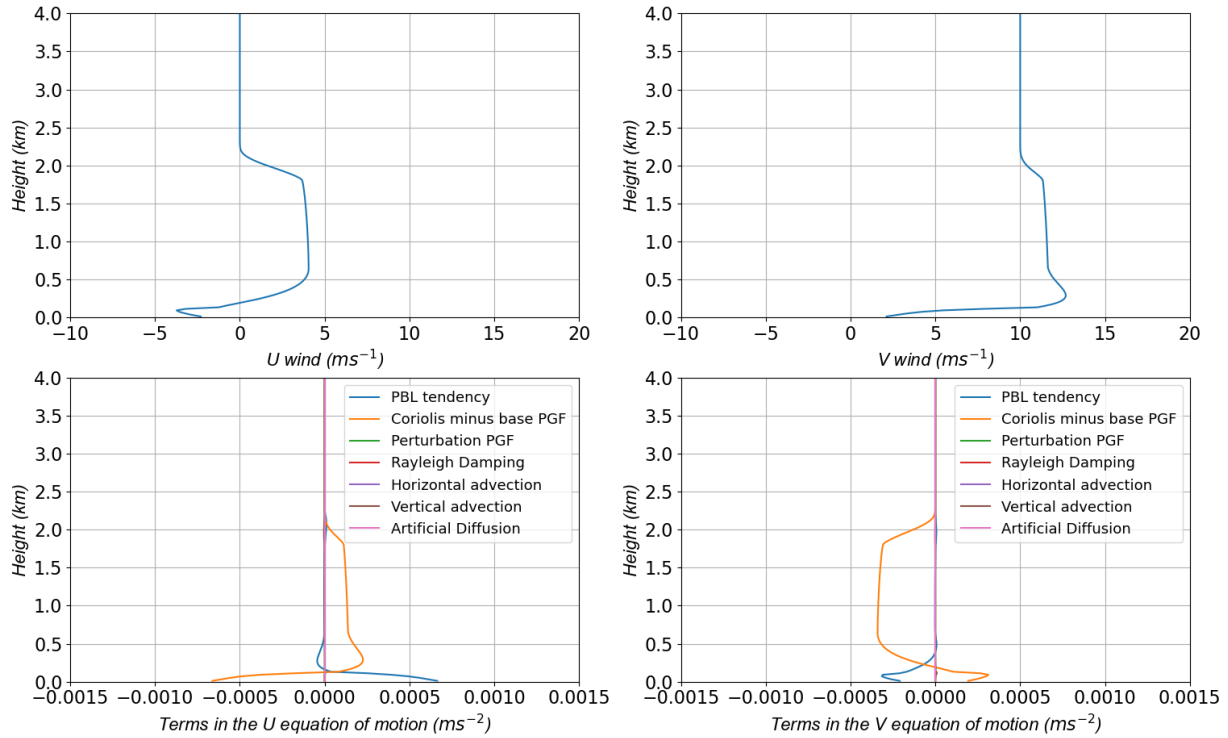
Figure 7. U wind (top left panel), V wind (top right panel), terms in the U equation of motion (bottom left panel) and terms in the V equation of motion (bottom right panel) at 0330 LST of the third day of the reference Blackadar run. The curves in the bottom panels are: PBL tendency (blue), Coriolis minus base PGF (orange), Perturbation PGF (green), Rayleigh Damping (red), Horizontal advection (purple), Vertical advection (brown) and Artificial diffusion (pink). The "PBL tendency" term represents the influence of turbulence in the U and V wind fields by the boundary layer scheme.
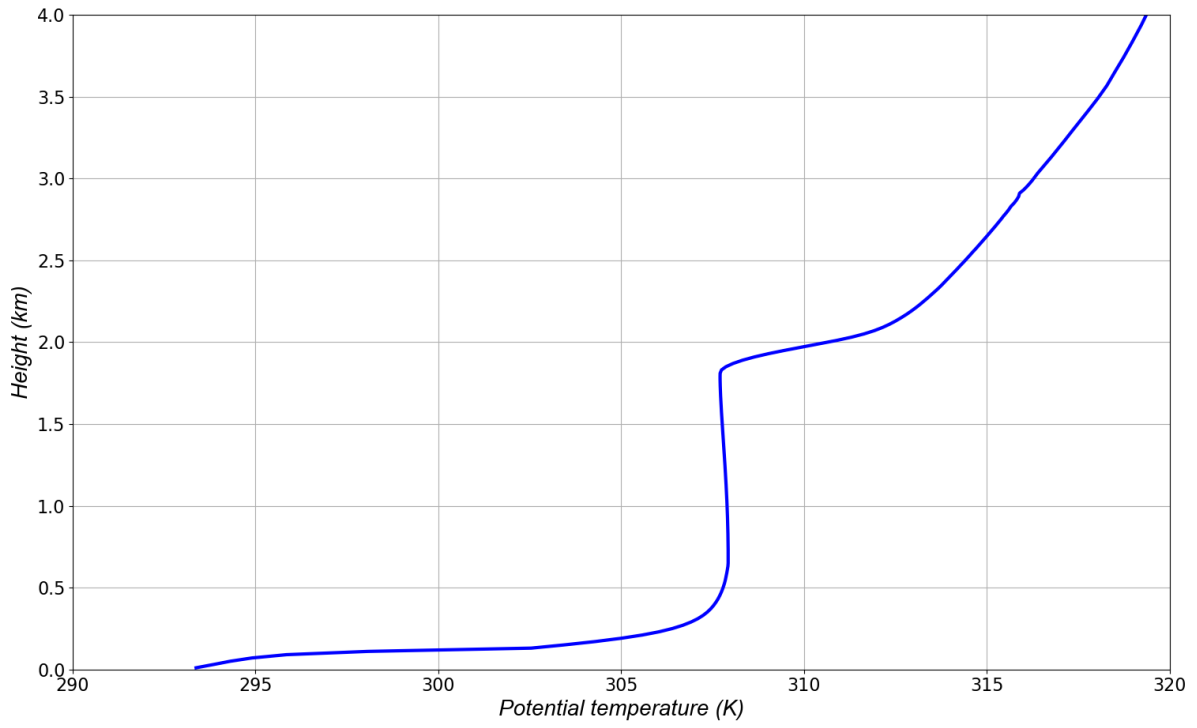
Figure 8. Potential temperature profile at 0330 LST of the third day of the reference Blackadar run.
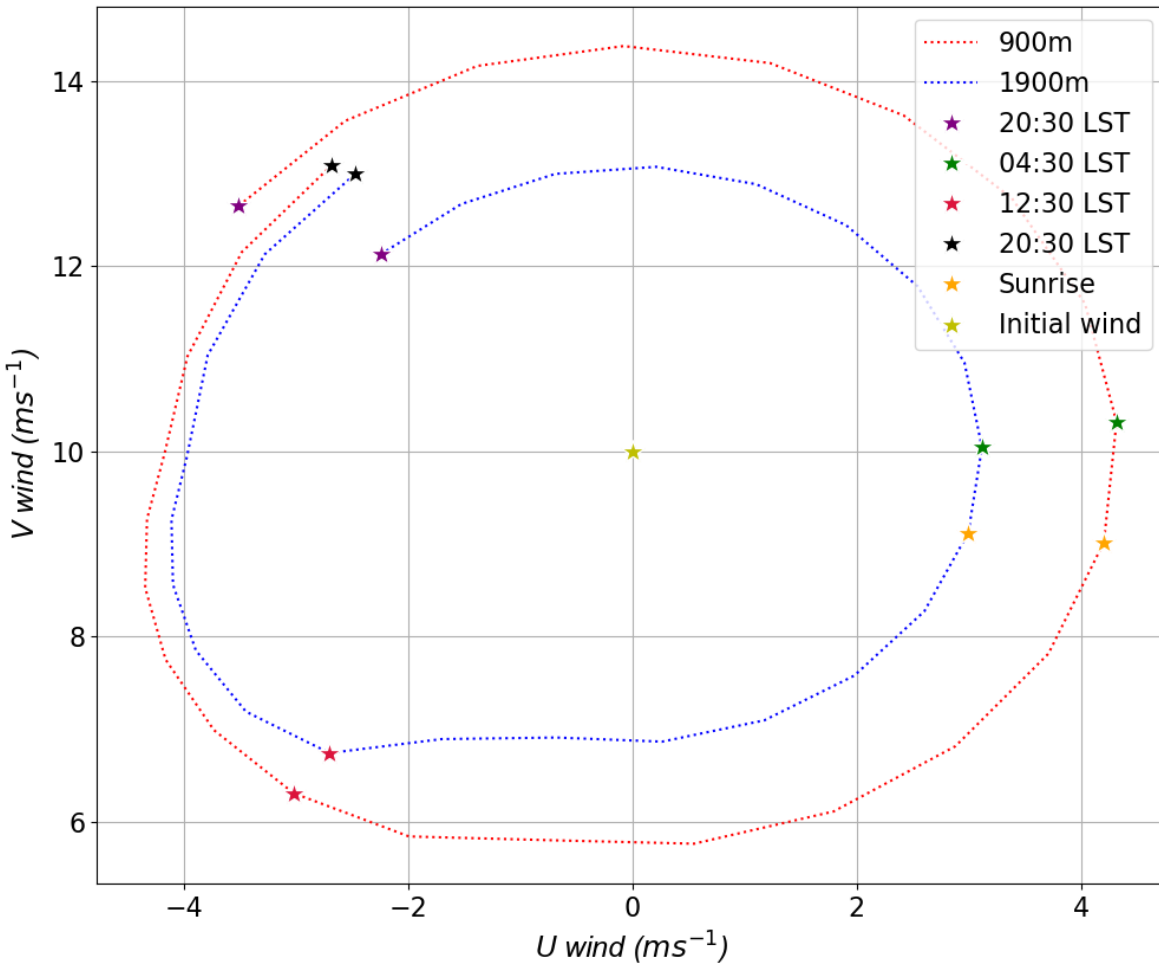
Figure 9. Plot of the evolution of the U and V components of the wind at 900 m and 1900 m starting at 2030 LST (sunset) of the second day (purple star) and ending at 2030 LST of the third day of the reference Blackadar run (black star).
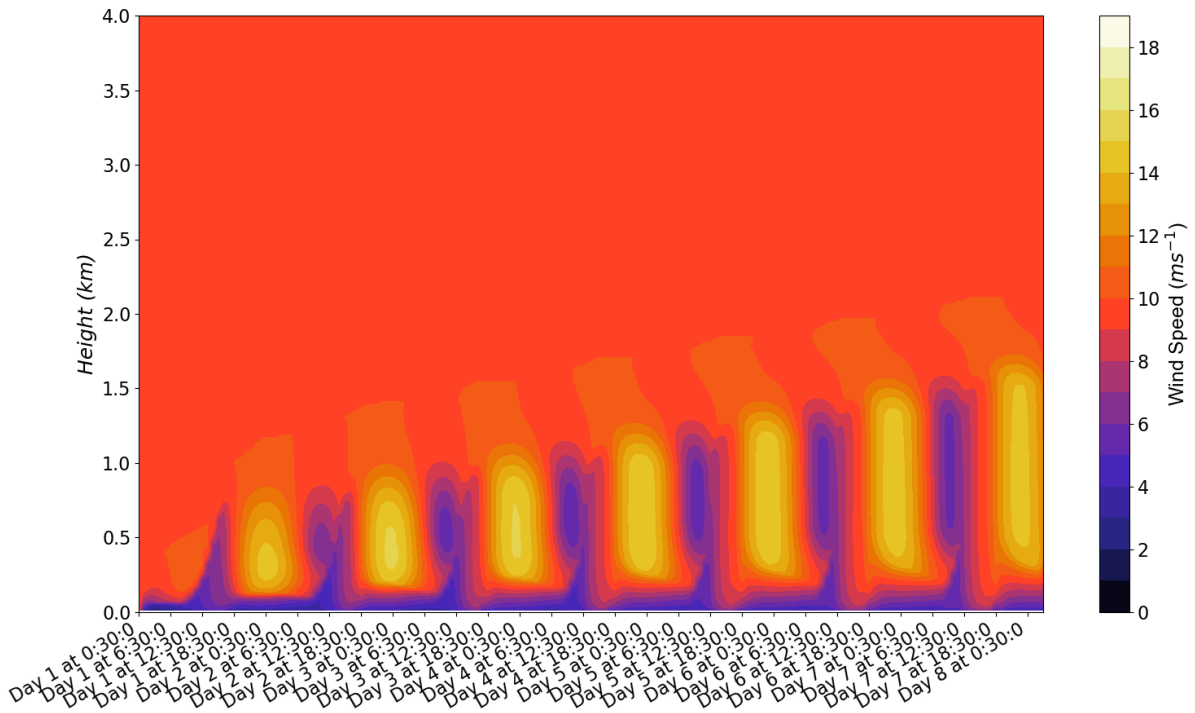
Figure 10. Same as figure 4, but for the reference run with a starting date of February 10th.
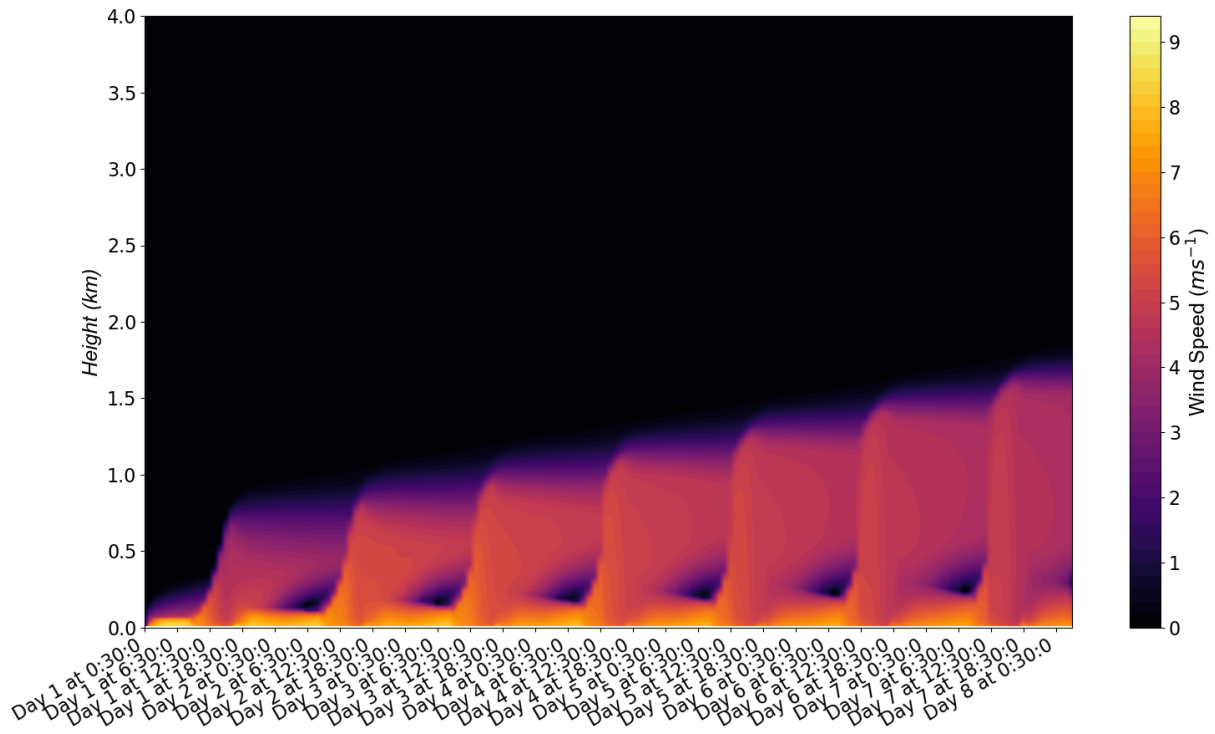
Figure 11. Same as figure 6, but for the reference run with a starting date of February 10th.
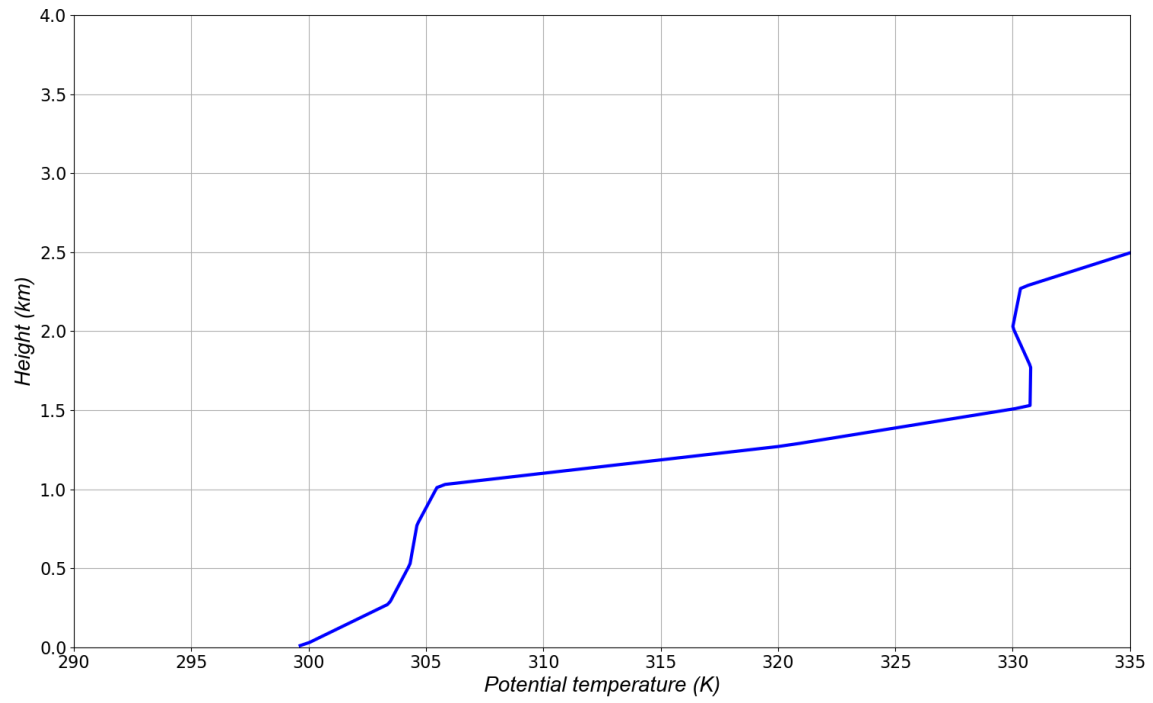
Figure 12. Initial profile of potential temperature for the reference run with a very strong inversion.
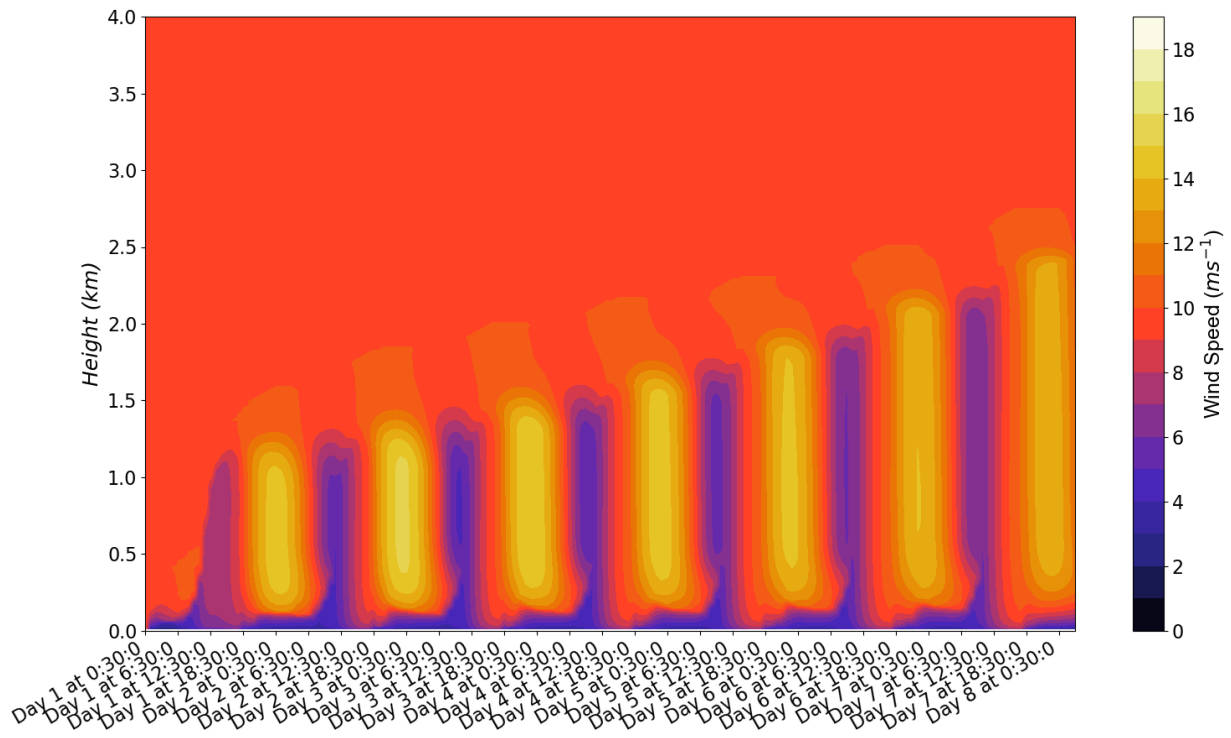
Figure 13. Same as figure 4, but for the reference run with a very strong inversion.
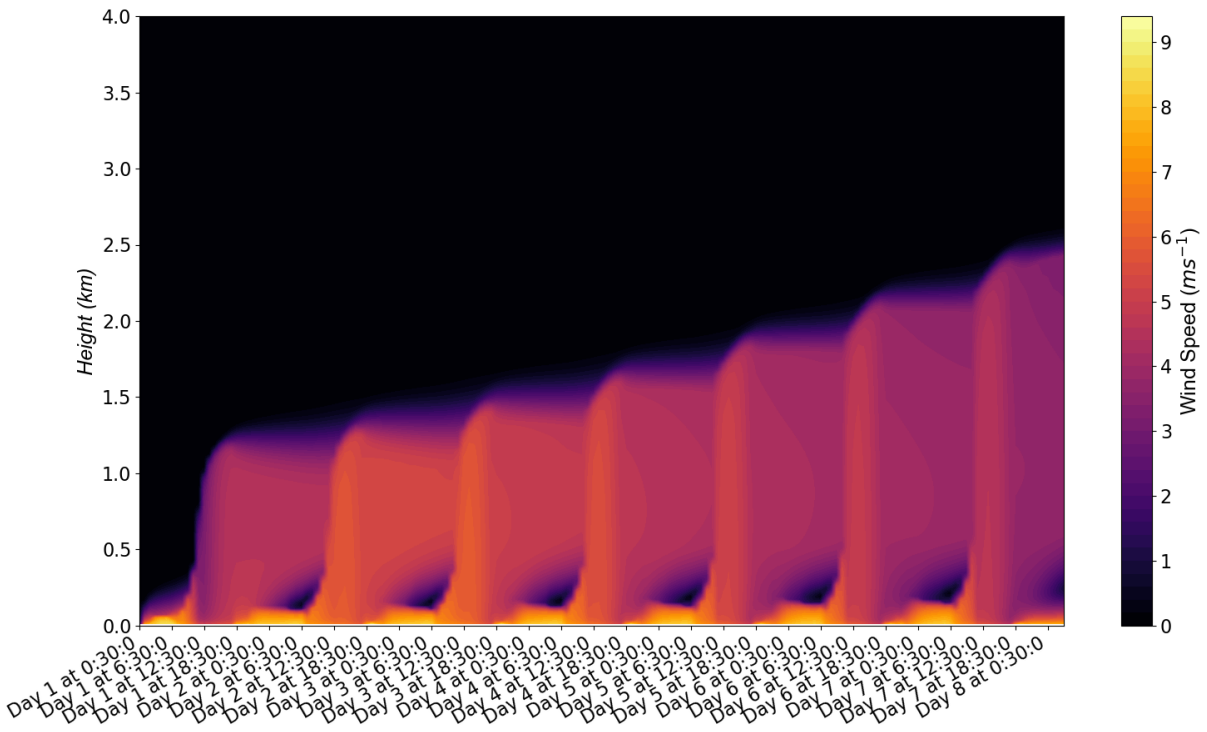
Figure 14. Same as figure 6, but for the reference run with a very strong inversion.
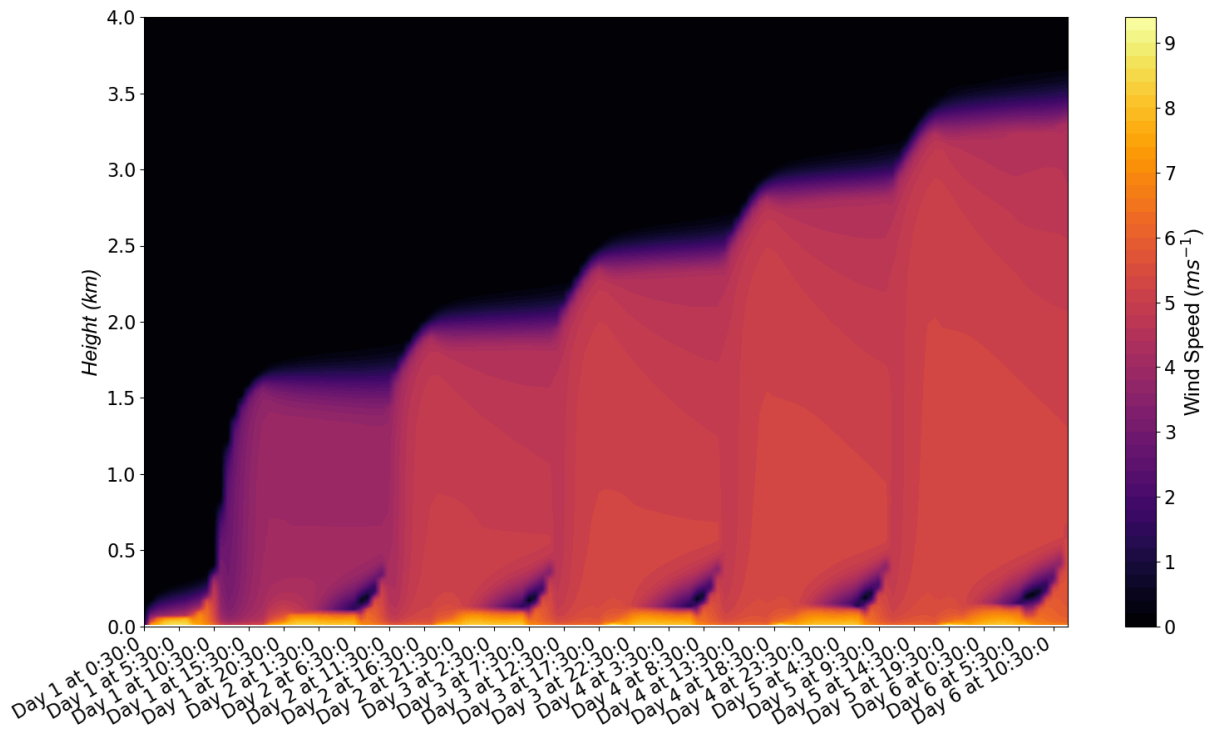
Figure 15. Same as figure 6, but for the reference run conducted at 30ºN.
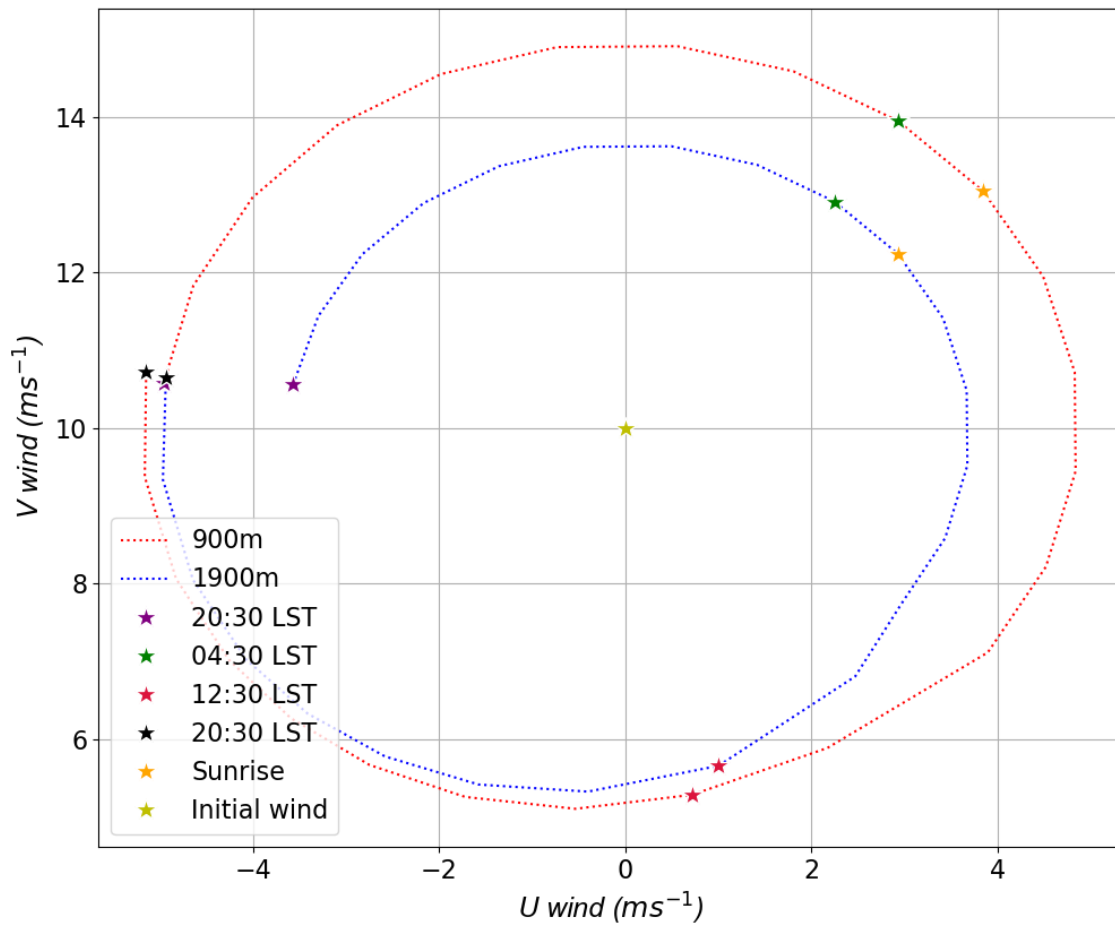
Figure 16. Same as in figure 9, but for the reference run conducted at 30ºN.
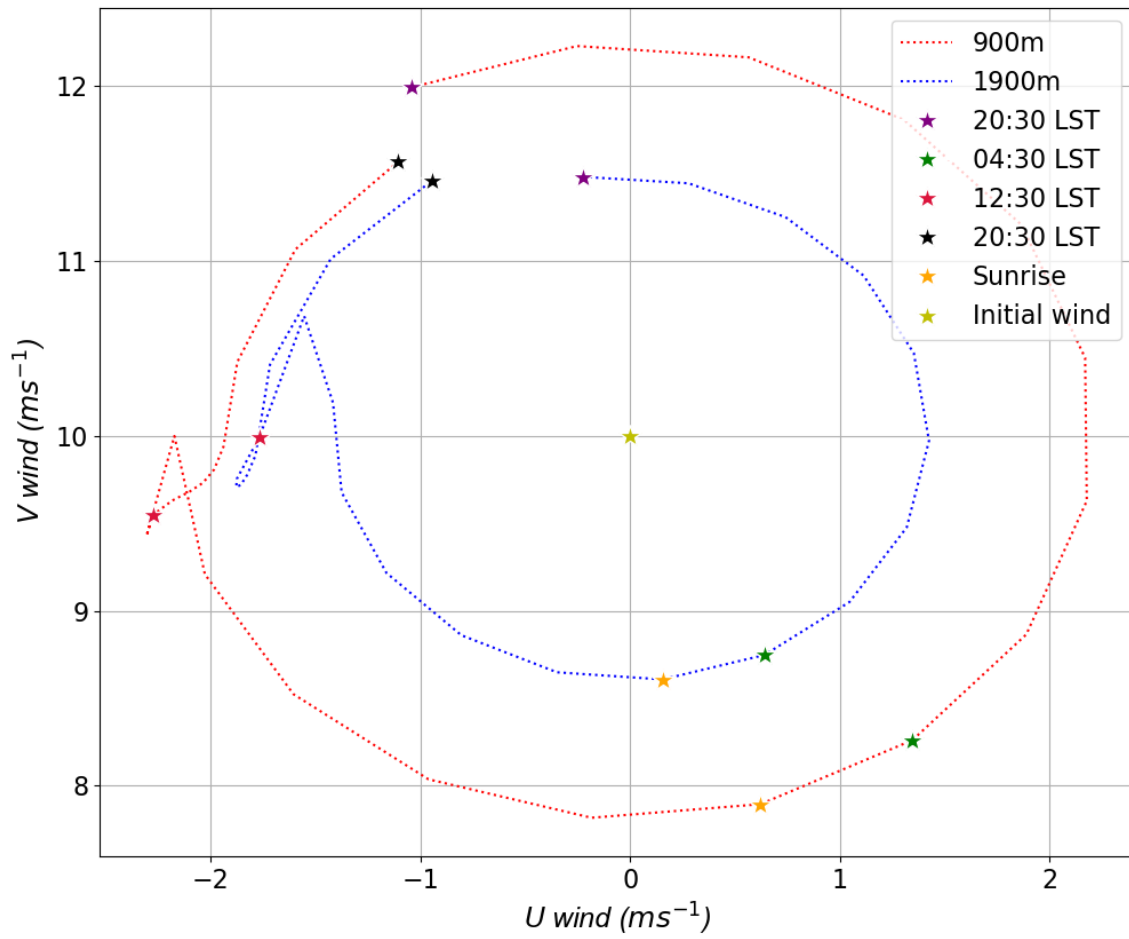
Figure 17. Same as in figure 9, but for the reference run conducted at 45ºN.
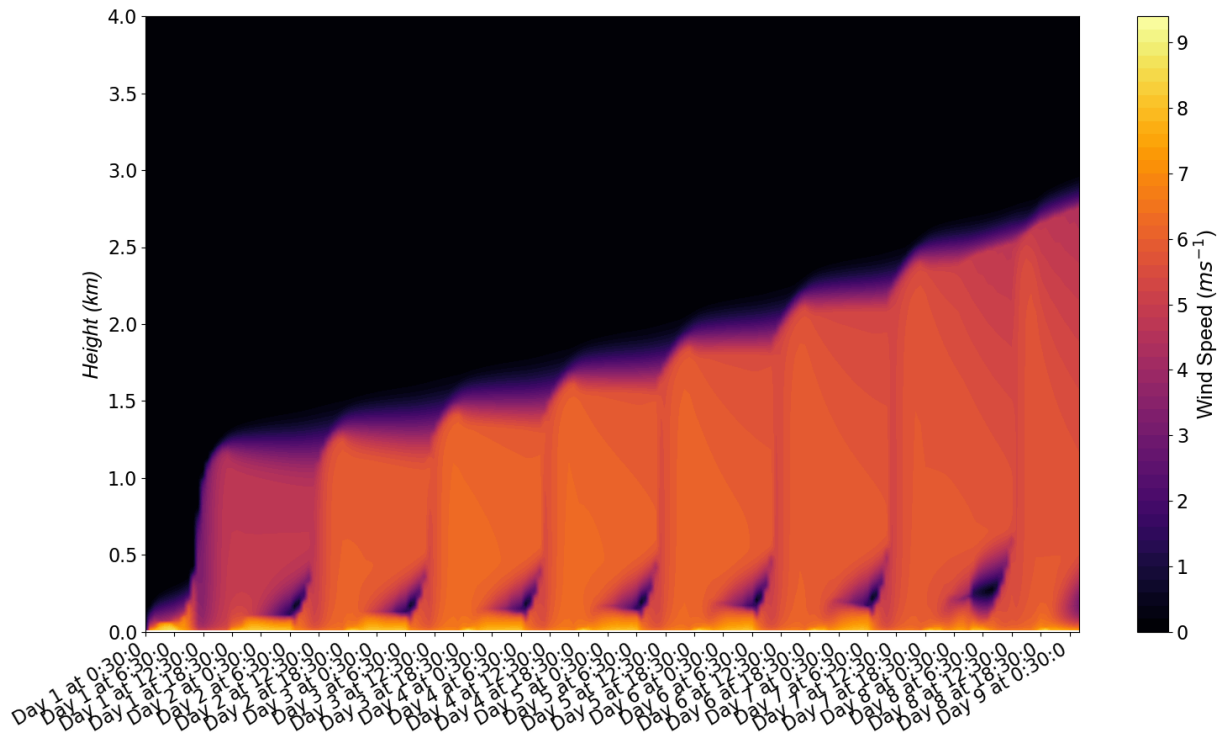
Figure 18. Same as figure 6, but for the reference run conducted at 30ºN with a very strong inversion.
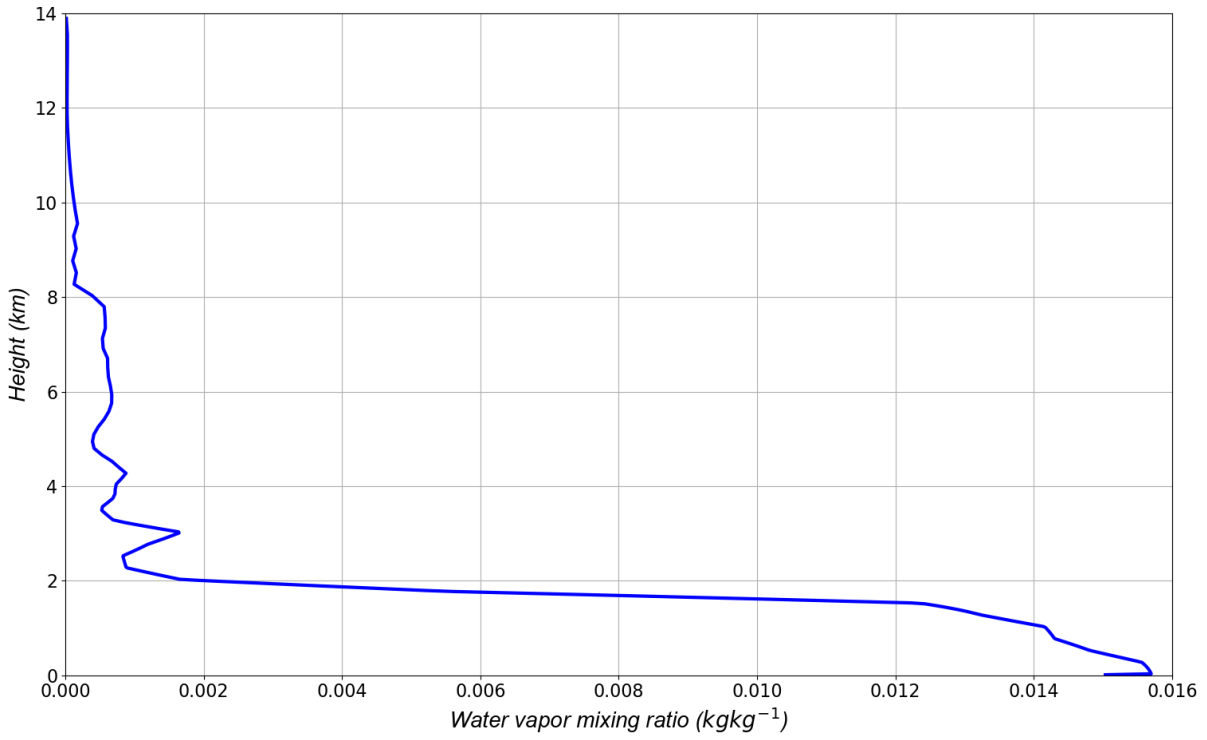
Figure 19. Initial moisture profile in the reference Blackadar jet run with modified moisture profile.
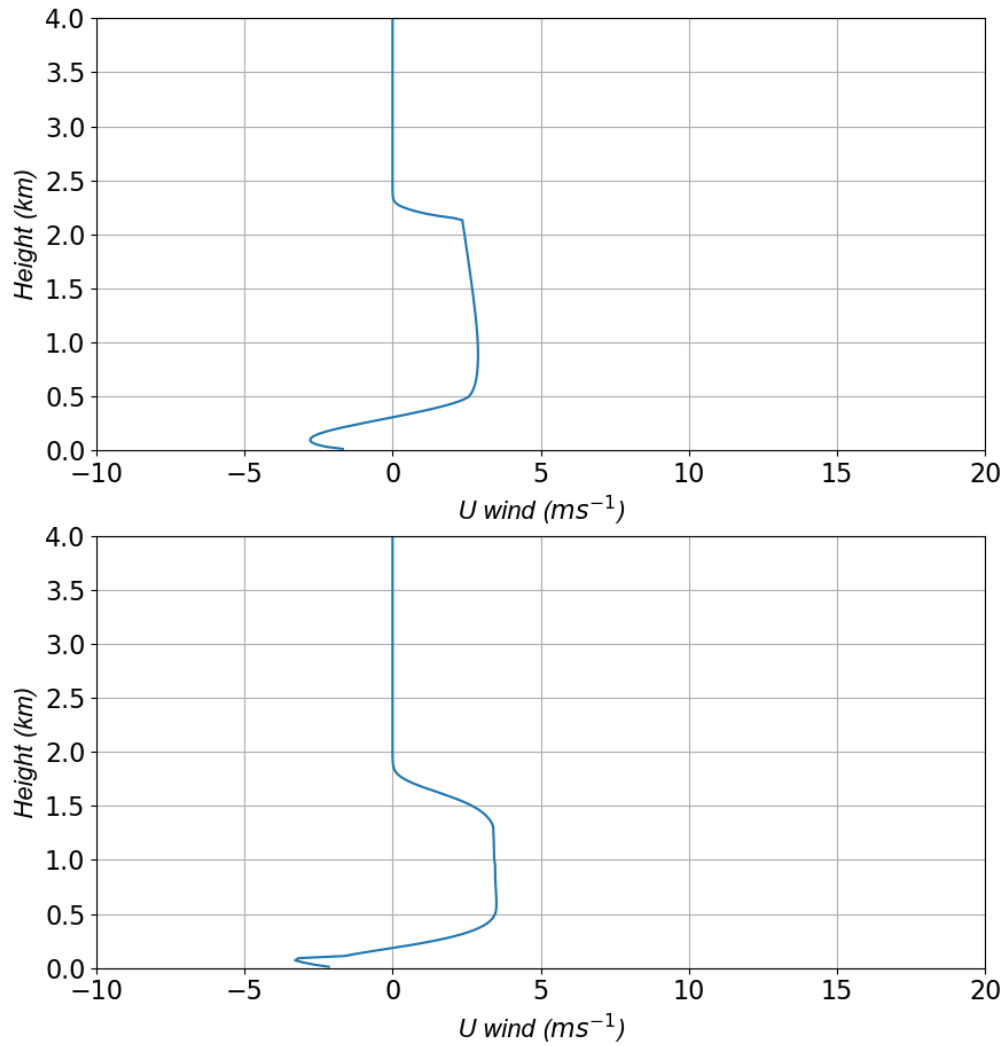
Figure 20. U wind profile for the reference Blackadar run with modified moisture profile (top panel) and for the reference Blackadar run (bottom panel) in the second day of the simulations at 0430 LST (of both simulations).
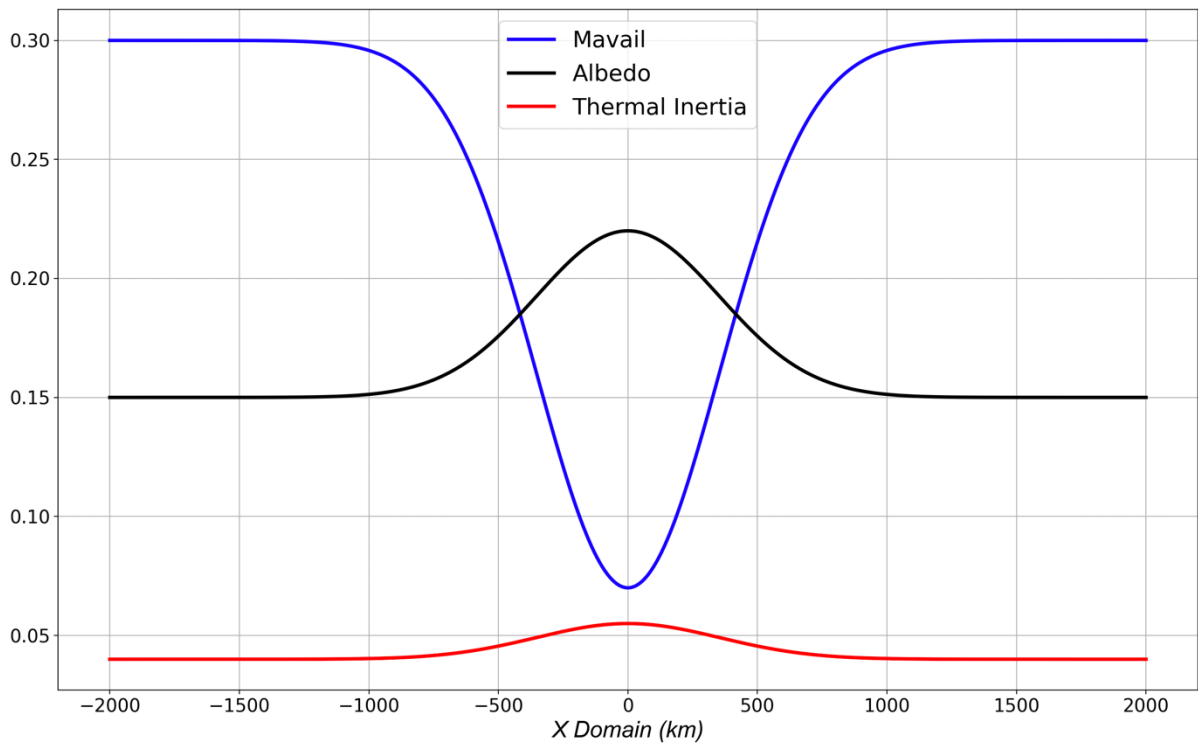
Figure 21. Values of MAVAIL (blue), albedo (black) and thermal inertia (red) for every value of x.
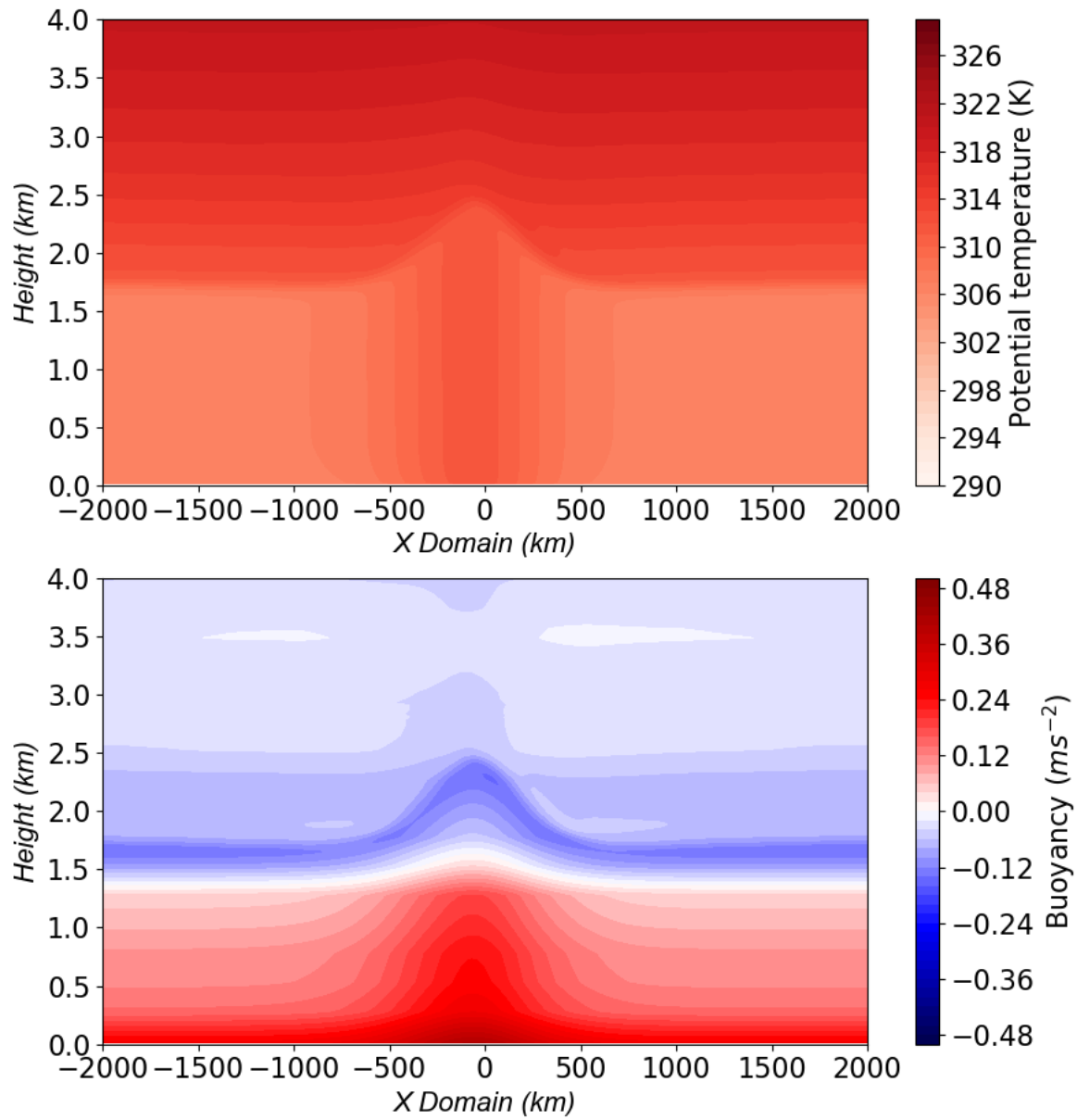
Figure 22. Potential temperature (top panel) and buoyancy (bottom panel) in the second day of the reference baroclinic run at 1830 LST.
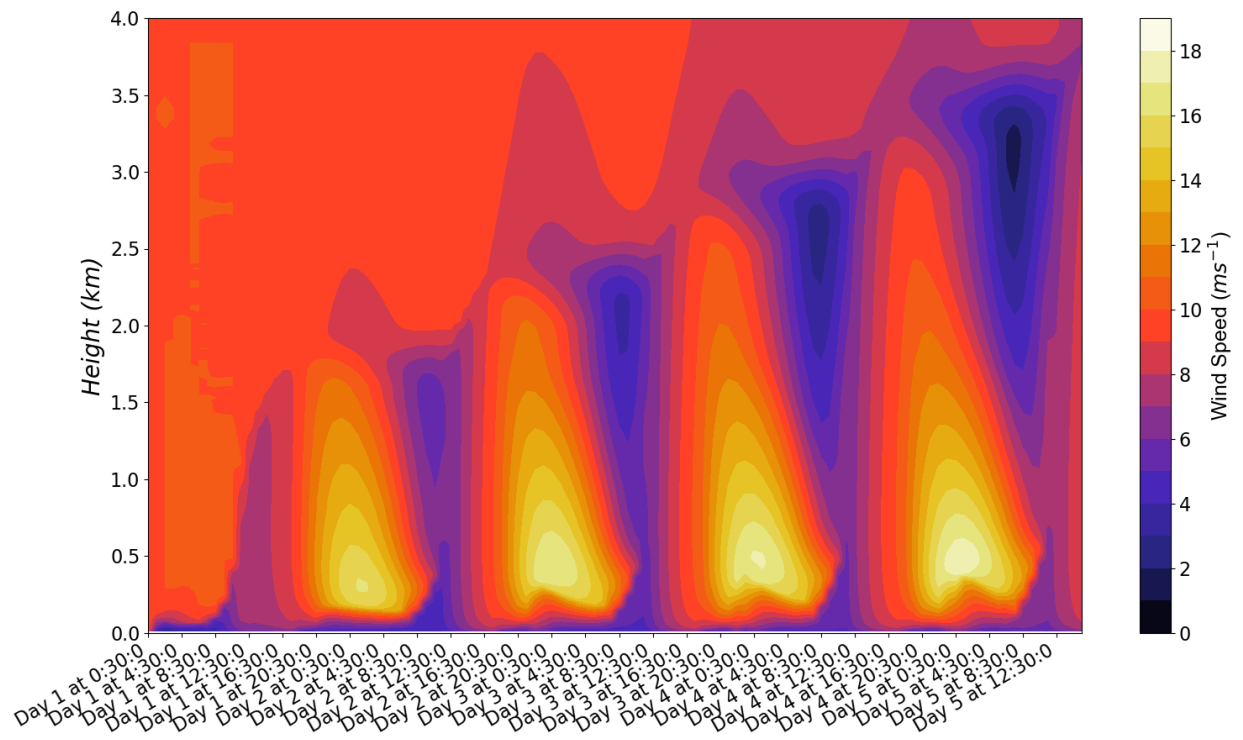
Figure 23. Wind speed as a function of time and height for a location 90 km east of the center of the domain in the reference baroclinic run.
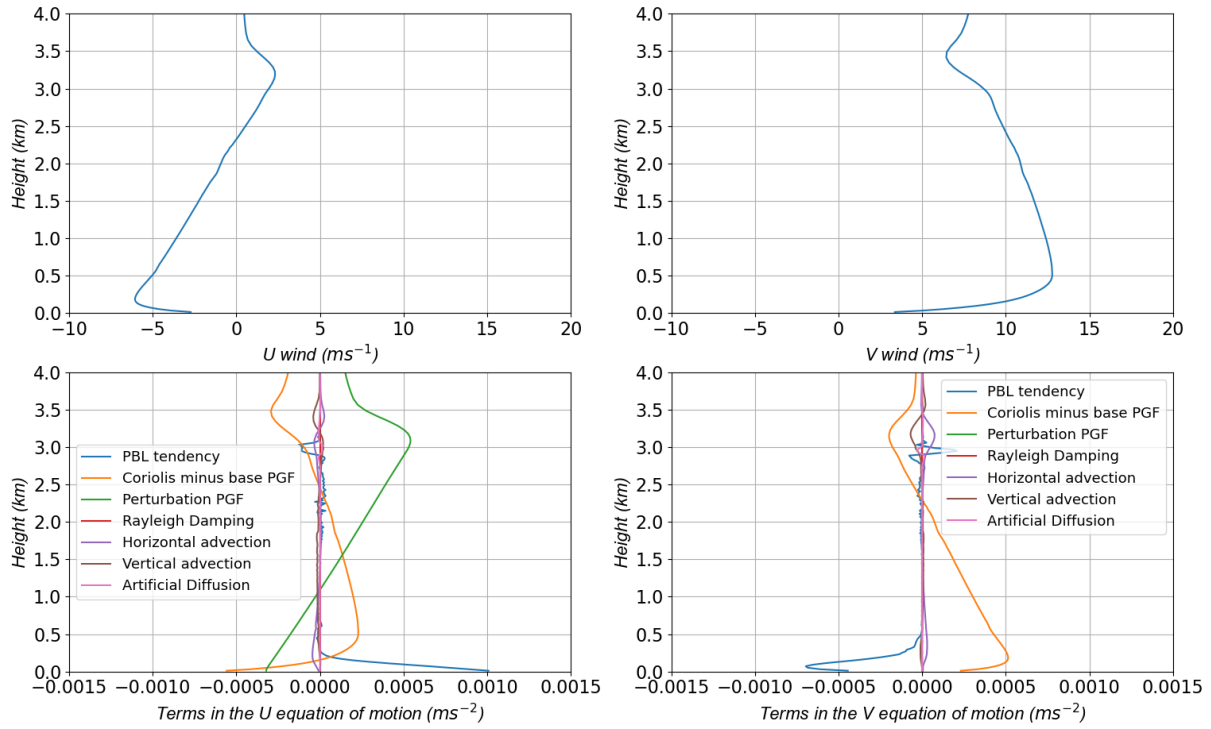
Figure 24. Same as figure 7 but for the reference baroclinic jet run. The profiles are for a location 90 km east of the center of the domain in the fourth day of the simulation at 2030 LST.
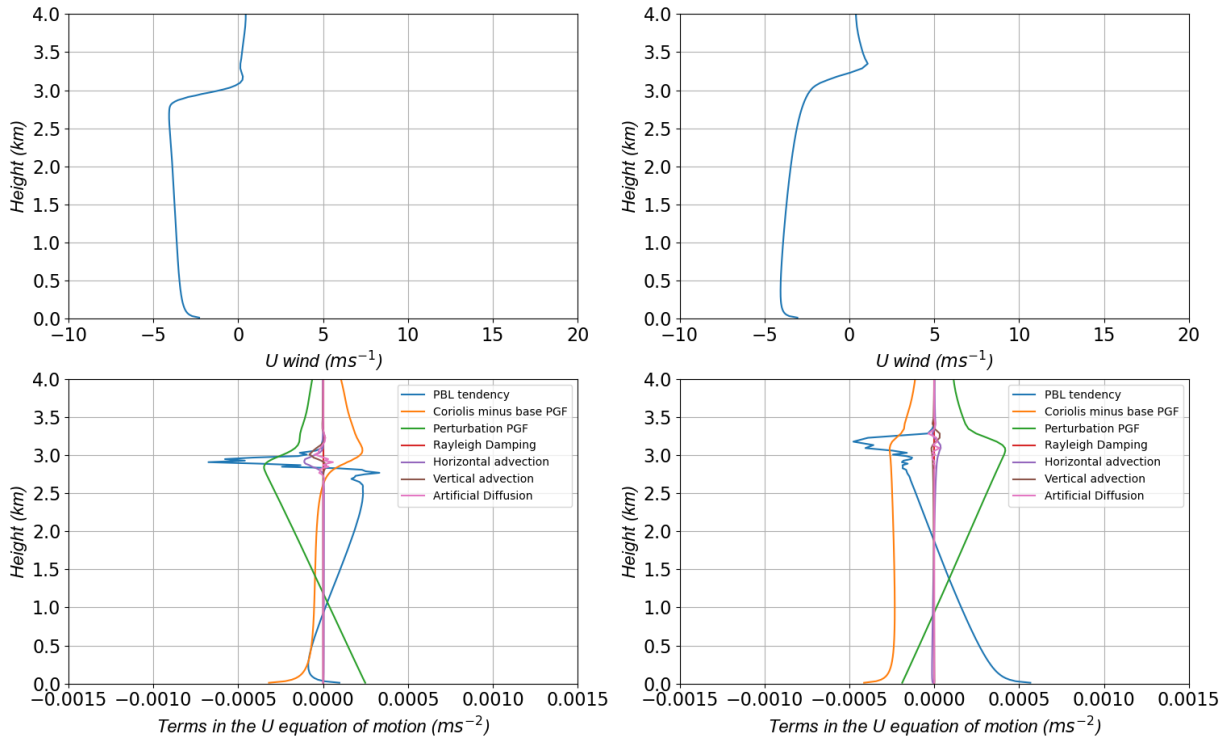
Figure 25. Similar to figure 7 but for the reference baroclinic jet run. All the profiles are for the fourth day of the simulation at 1430 LST. The panels in the right side represent a location 90 km to the right the center of the domain and the panels in the left represent a location 270 km to the left of the center of the domain. Because the center of the warm tongue and the center of the peak vertical motion are slightly shifted to the west due to advection, these two locations are not symmetric with respect to the center of the domain. The U wind profiles in the top panels indicate that there should be convergence in the center of the domain approximately from the surface to 1.5 km and divergence from 1.5 km to 3 km.
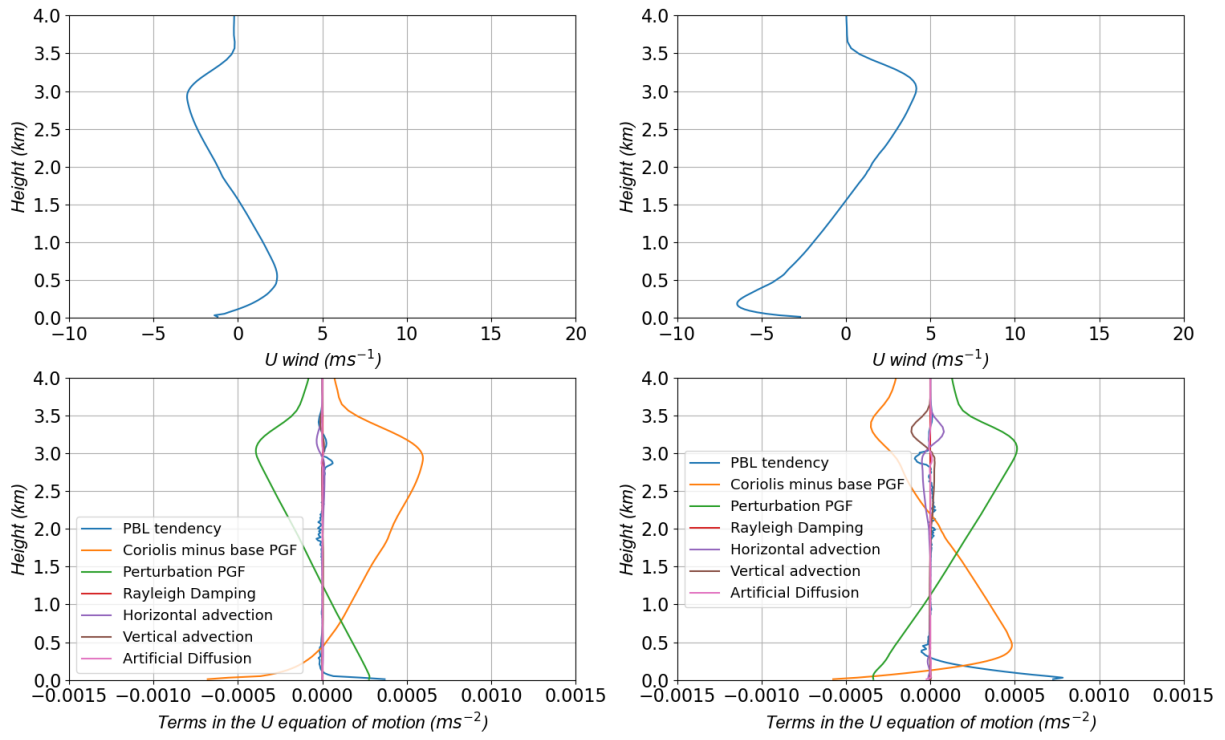
Figure 26. Same as figure 25 but 8 hours later.
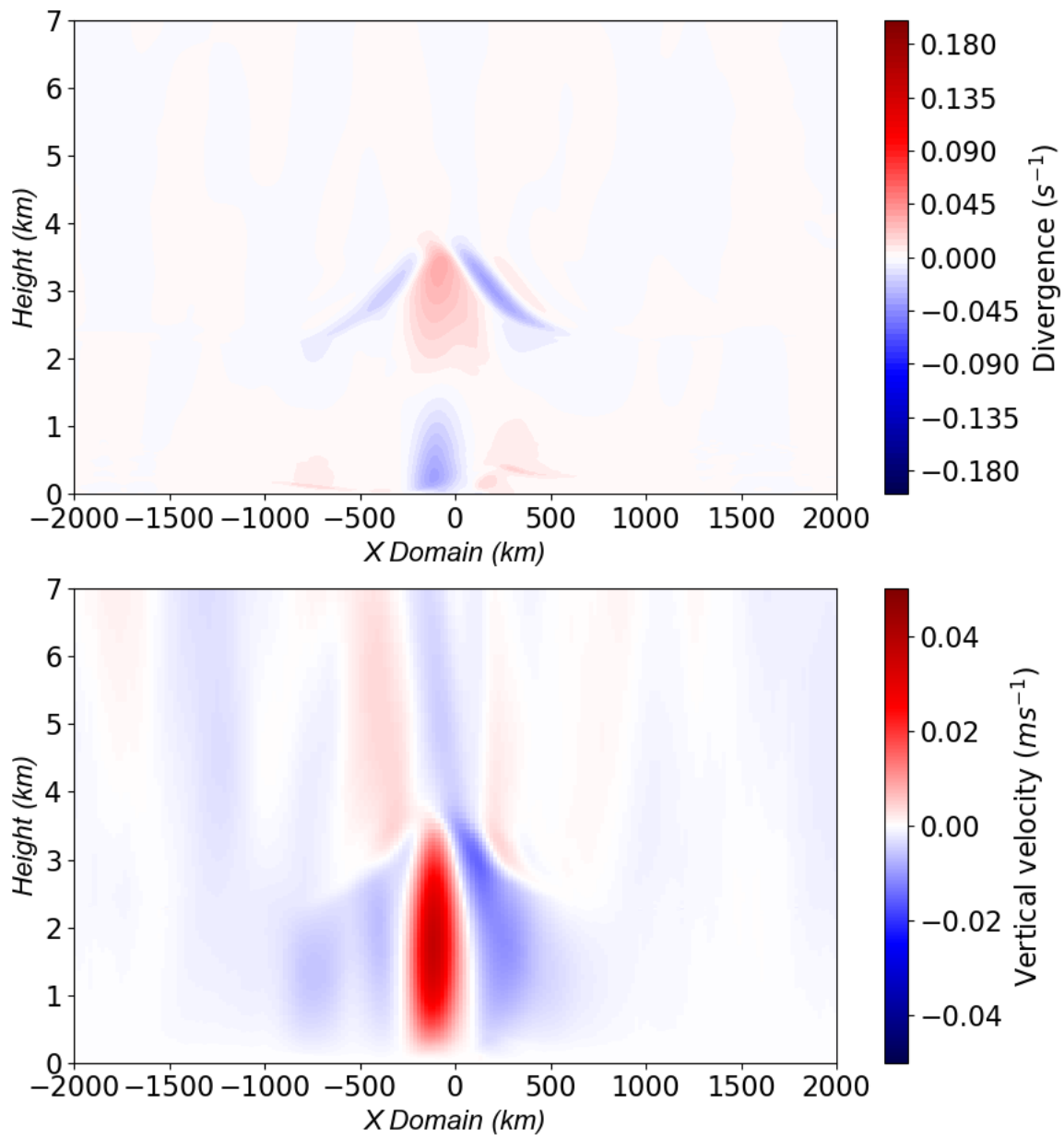
Figure 27. Divergence (top panel) and vertical motion (bottom panel) at 2230 LST of the fourth day of the reference baroclinic jet run.
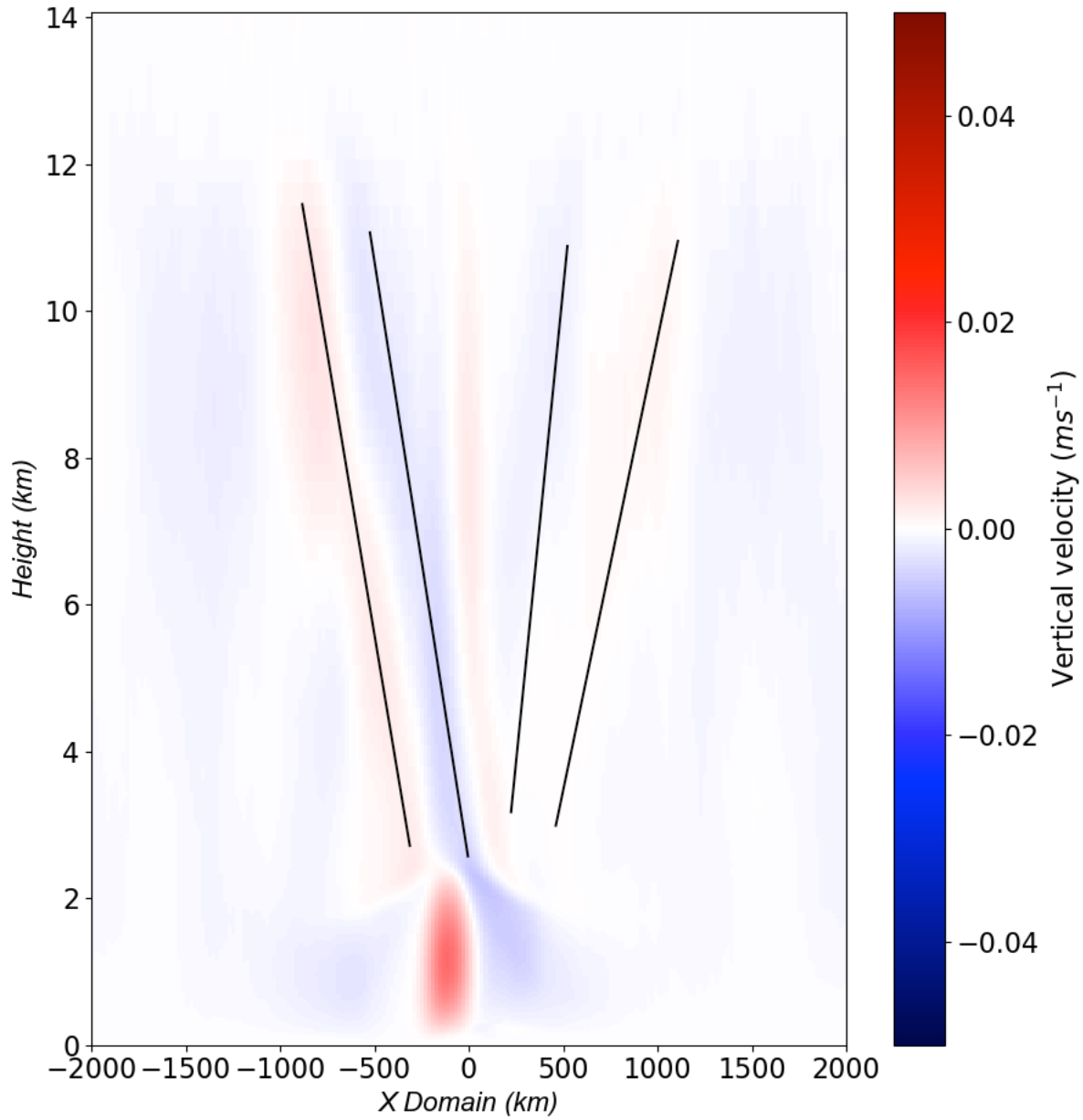
Figure 28. Vertical motion at 2330 LST of the second day of the reference baroclinic jet run. The propagation of the phase fronts is perpendicular to the phase lines (in black) and pointing outwards from the center of the domain. Only four of the phase lines are indicated in the figure.
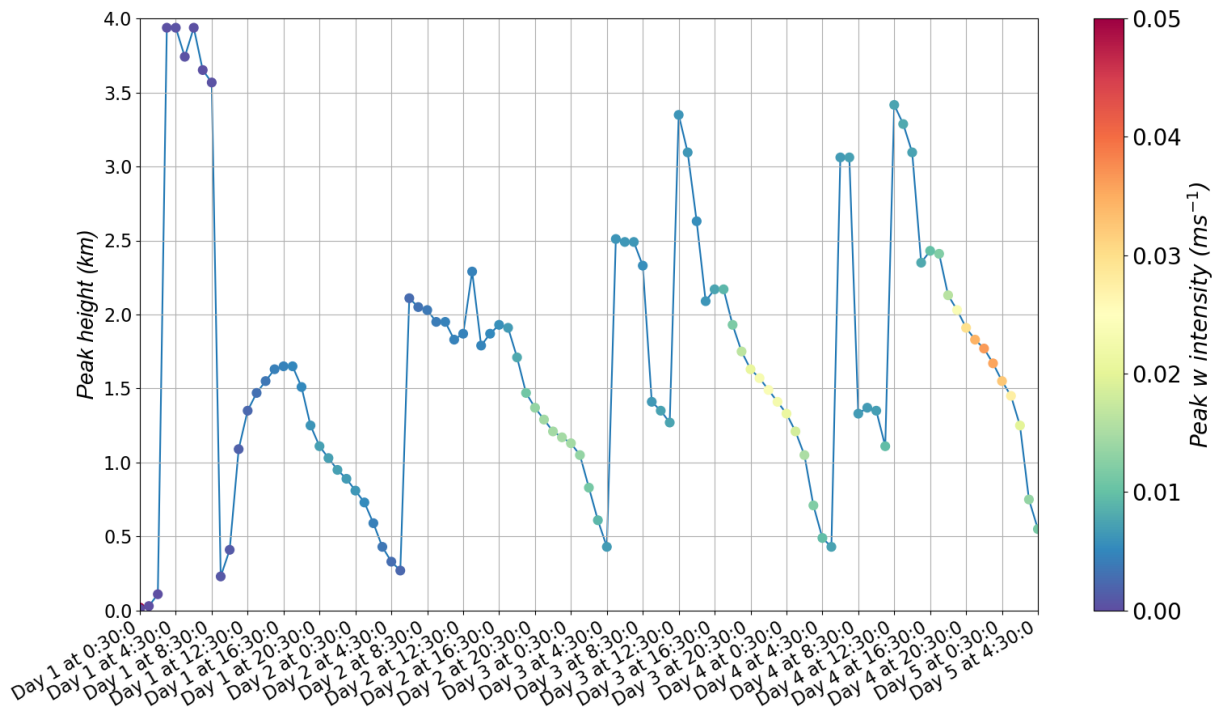
Figure 29. Height of the strongest W in the lowest 4 km of the domain for each hour of the reference baroclinic jet run.
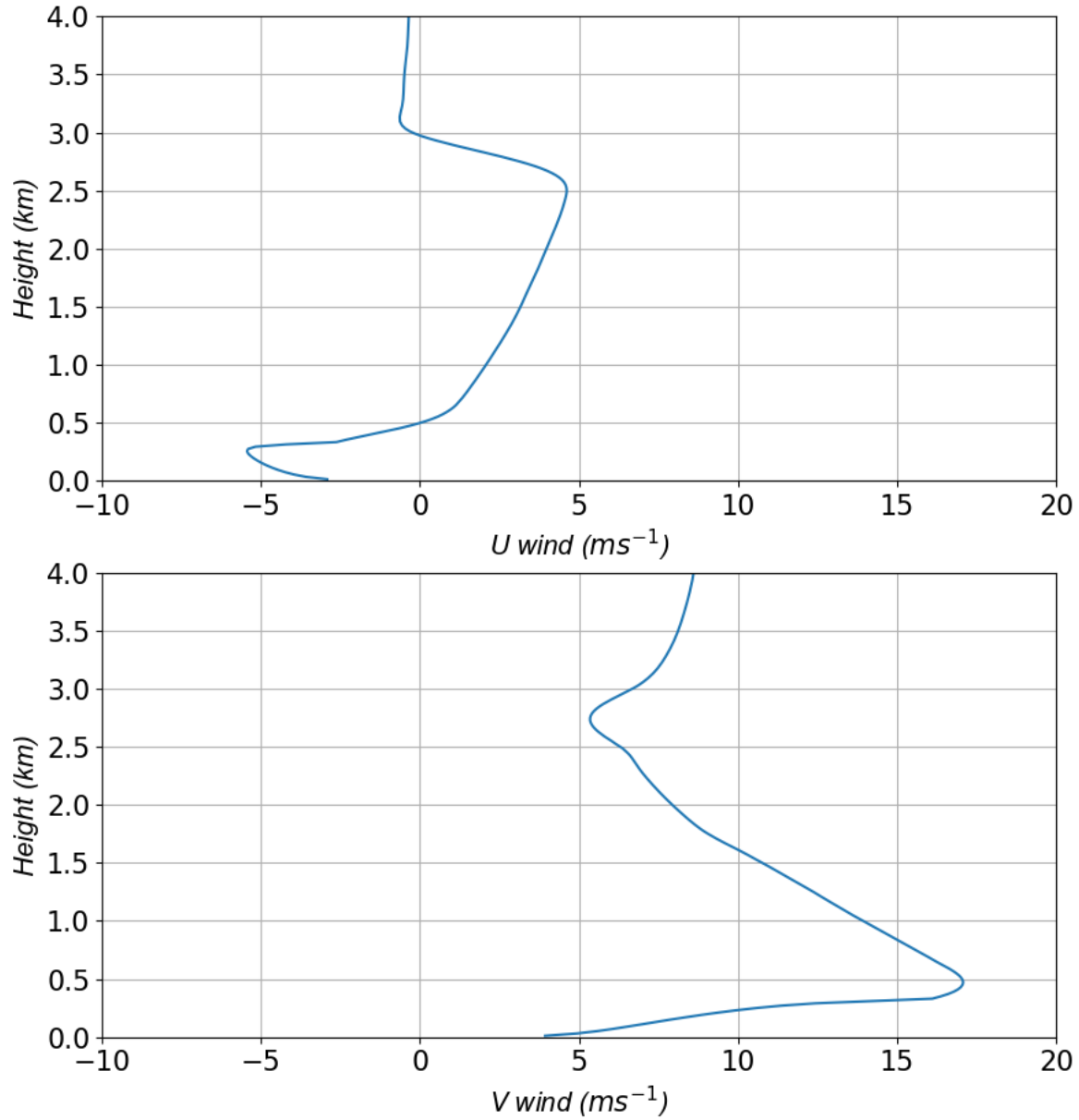
Figure 30. U wind profile (top) and V wind profile (bottom) for the reference baroclinic run in the fourth day of the simulation at 0130 LST. Both profiles are for a location 90 km to the right of the center of the domain.
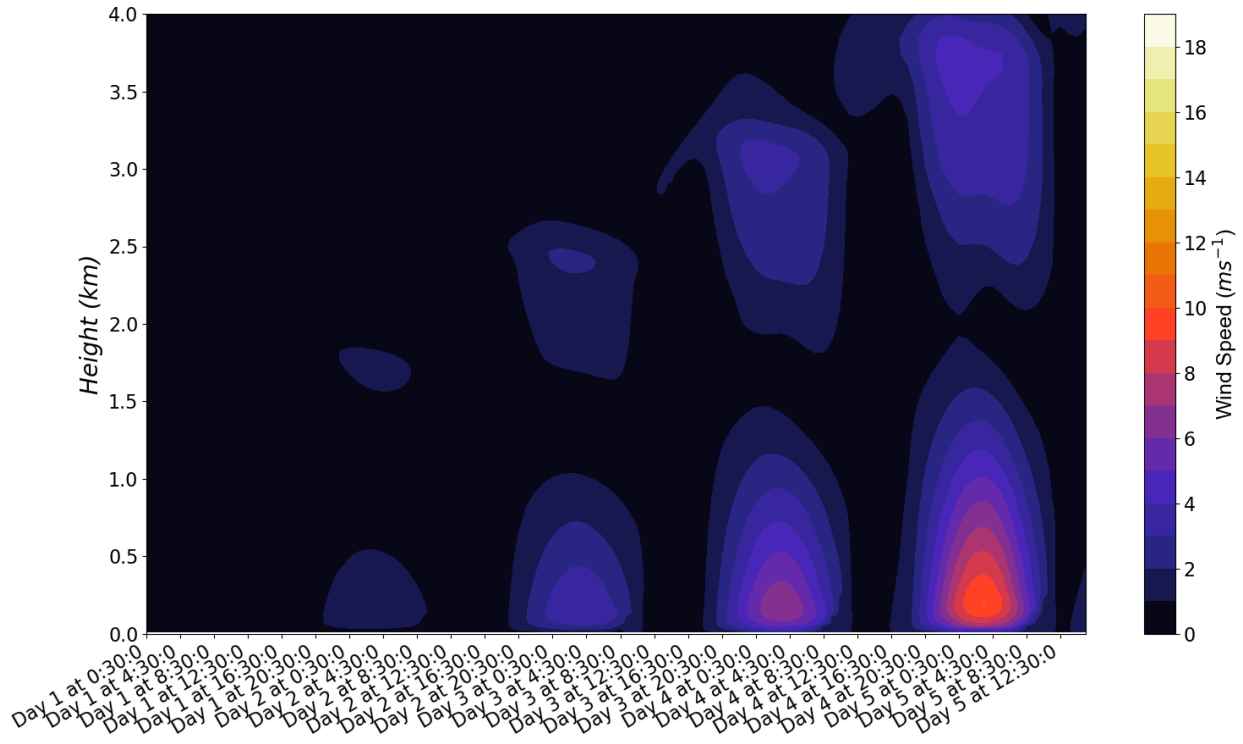
Figure 31. Same as in figure 23 but for the reference baroclinic jet run with no initial geostrophic wind.
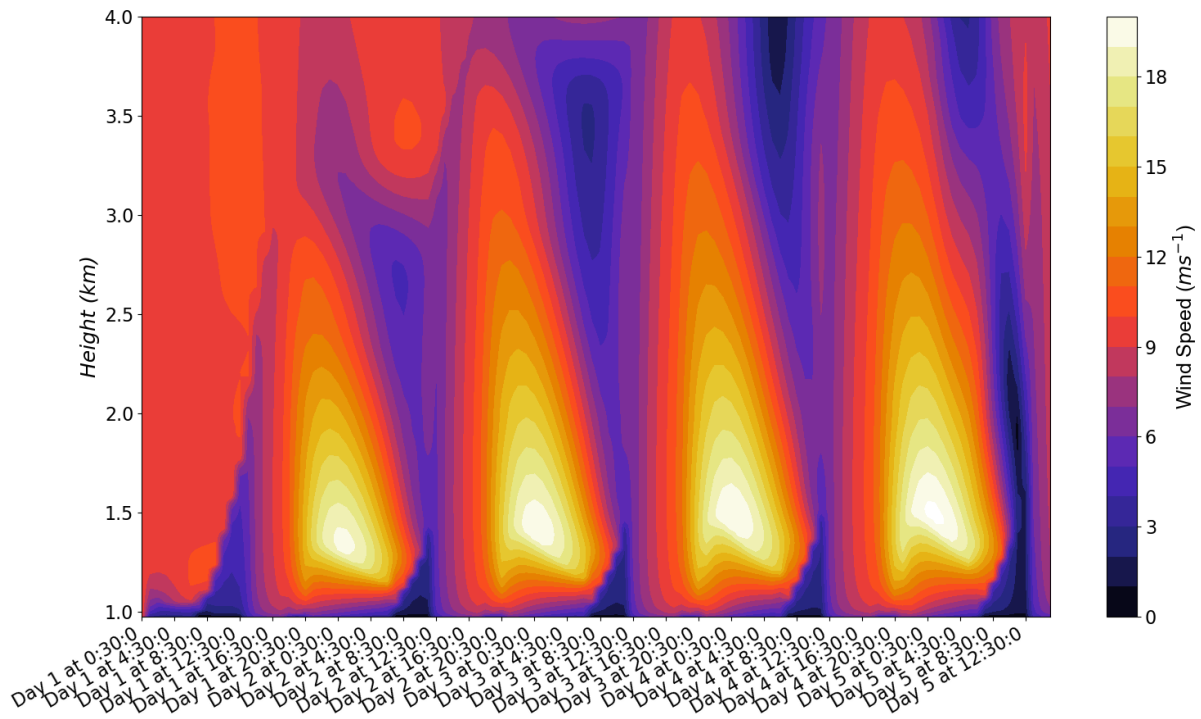
Figure 32. Same as in figure 23 but for the reference baroclinic run with hill shaped terrain. The plot starts at 977 m, which is the terrain height at the location (still 90 km to the east of the domain center) chosen to create this plot.
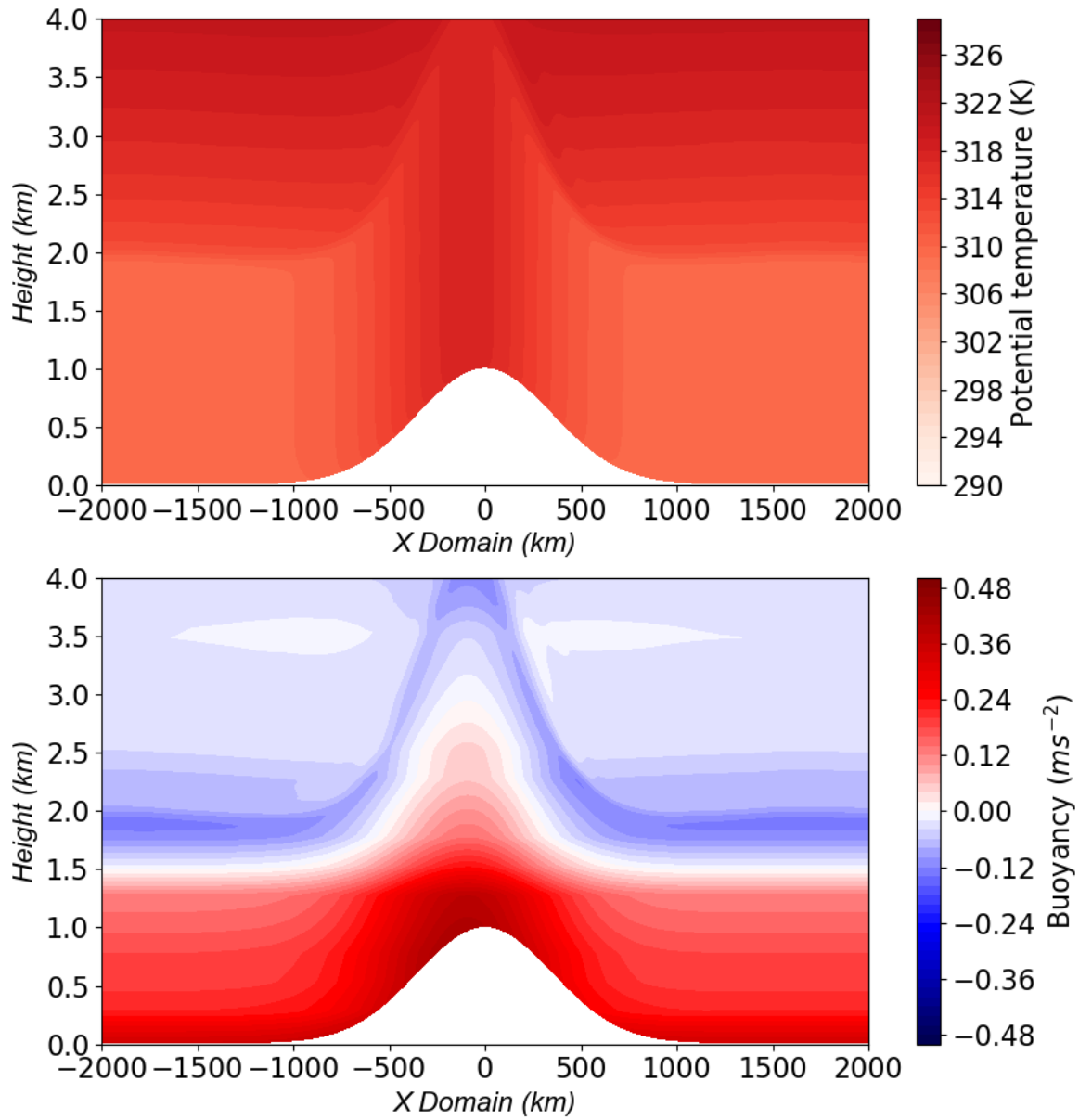
Figure 33. Same as figure 22, but for the reference baroclinic run with hill shaped terrain.